Autophagy

Volume 11 • Issue 11 • November 2015

Editor-in-Chief
Daniel J. Klionsky
University of Michigan

Taylor & Francis
Taylor & Francis Group

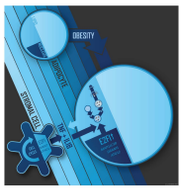

Autophagy

ISSN: (Print) (Online) Journal homepage: https://www.tandfonline.com/loi/kaup20

MoVast2 combined with MoVast1 regulates lipid homeostasis and autophagy in *Magnaporthe oryzae*

Xue-Ming Zhu, Lin Li, Jian-Dong Bao, Jiao-Yu Wang, Shuang Liang, Li-Li Zhao, Chang-Li Huang, Jiong-Yi Yan, Ying-Ying Cai, Xi-Yu Wu, Bo Dong, Xiao-Hong Liu, Daniel J. Klionsky & Fu-Cheng Lin

To cite this article: Xue-Ming Zhu, Lin Li, Jian-Dong Bao, Jiao-Yu Wang, Shuang Liang, Li-Li Zhao, Chang-Li Huang, Jiong-Yi Yan, Ying-Ying Cai, Xi-Yu Wu, Bo Dong, Xiao-Hong Liu, Daniel J. Klionsky & Fu-Cheng Lin (2023): MoVast2 combined with MoVast1 regulates lipid homeostasis and autophagy in *Magnaporthe oryzae*, Autophagy, DOI: 10.1080/15548627.2023.2181739

To link to this article: https://doi.org/10.1080/15548627.2023.2181739

AUTOPHAGY
https://doi.org/10.1080/15548627.2023.2181739

Taylor & Francis
Taylor & Francis Group

RESEARCH PAPER

MoVast2 combined with MoVast1 regulates lipid homeostasis and autophagy in *Magnaporthe oryzae*

Xue-Ming Zhu[a], Lin Li[a], Jian-Dong Bao[a], Jiao-Yu Wang[a], Shuang Liang[a], Li-Li Zhao[a], Chang-Li Huang[a], Jiong-Yi Yan[b], Ying-Ying Cai[b], Xi-Yu Wu[b], Bo Dong[c], Xiao-Hong Liu[b], Daniel J. Klionsky[d], and Fu-Cheng Lin[a,b]

[a]State Key Laboratory for Managing Biotic and Chemical Treats to the Quality and Safety of Agro-products, Institute of Plant Protection and Microbiology, Zhejiang Academy of Agricultural Sciences, Hangzhou, Zhejiang, China; [b]State Key Laboratory of Rice Biology, Institute of Biotechnology, Zhejiang University, Hangzhou, Zhejiang, China; [c]Markey Cancer Center, University of Kentucky, College of Medicine, Lexington, KY, USA; [d]Life Sciences Institute and Department of Molecular, Cellular and Developmental Biology, University of Michigan, Ann Arbor, MI, USA

ABSTRACT

Macroautophagy/autophagy is an evolutionarily conserved biological process among eukaryotes that degrades unwanted materials such as protein aggregates, damaged mitochondria and even viruses to maintain cell survival. Our previous studies have demonstrated that MoVast1 acts as an autophagy regulator regulating autophagy, membrane tension, and sterol homeostasis in rice blast fungus. However, the detailed regulatory relationships between autophagy and VASt domain proteins remain unsolved. Here, we identified another VASt domain-containing protein, MoVast2, and further uncovered the regulatory mechanism of MoVast2 in *M. oryzae*. MoVast2 interacted with MoVast1 and MoAtg8, and colocalized at the PAS and deletion of *MoVAST2* results in inappropriate autophagy progress. Through TOR activity analysis, sterols and sphingolipid content detection, we found high sterol accumulation in the Δ*Movast2* mutant, whereas this mutant showed low sphingolipids and low activity of both TORC1 and TORC2. In addition, MoVast2 colocalized with MoVast1. The localization of MoVast2 in the *MoVAST1* deletion mutant was normal; however, deletion of *MoVAST2* leads to mislocalization of MoVast1. Notably, the wide-target lipidomic analyses revealed significant changes in sterols and sphingolipids, the major PM components, in the Δ*Movast2* mutant, which was involved in lipid metabolism and autophagic pathways. These findings confirmed that the functions of MoVast1 were regulated by MoVast2, revealing that MoVast2 combined with MoVast1 maintained lipid homeostasis and autophagy balance by regulating TOR activity in *M. oryzae*.

ARTICLE HISTORY
Received 27 September 2022
Revised 10 February 2023
Accepted 13 February 2023

KEYWORDS
Autophagy; lipid homeostasis; *magnaporthe oryzae*; regulation; TORC2

Introduction

The plasma membrane (PM) is the basis for the origin of cells and the continued survival of living cells, acting as a cell barrier and dynamic interface to selectively control the entry and exit of intracellular and extracellular substances, and also as a scaffolding platform for proteins to transmit signals [1,2]. In eukaryotes, the PM is mainly composed of lipids and proteins, including phospholipids, sterol lipids, a small amount of glycolipids and sphingolipids [3]. It has been confirmed that these lipids and proteins coordinate with each other to regulate PM homeostasis, which plays an important role in resisting the constantly changing environment [4,5]. The best-understood examples of coregulation are sphingolipids and sterols, which have a similar localization and cooperative activity in altering membrane order and nucleating lipid microdomains [6,7]. In yeast, loss of sterol biosynthesis-related genes *ERG2* and *ERG6* results in intense changes in sphingolipid levels [8]. In mammalian cells, lipoproteins such as OSBP and OSBPL5/ORP5, participate in both sterol and sphingolipid trafficking and cause accumulation of both lipids [9]. These functional interdependences suggested that there may be many genetic interactions between sphingolipid- and sterol-related genes [10].

The balance of sterols and sphingolipids of PM exert crucial roles in the maintenance of lipid homeostasis, which is controlled by TORC2-Ypk1 signaling [11–13]. In yeast, inactivation of TORC2 decreases the phosphorylation level of Ypk1 and reduces sphingolipid levels in the PM. Inhibition of sphingolipid synthesis or treatment by hypotonicity can lead to an increase in PM tension and the movement of Slm proteins from eisosomes to the membrane compartment containing TORC2 (MCT) regions, leading to activation of TORC2 signaling to promote sphingolipid biosynthesis [1,14,15]. Although the mechanism by which Slm proteins regulate PM tension through this relocation is unclear, the re-increase in cell membrane tension through activation of TORC2 is prevalent in mammalian cells and fungal yeast cells [16].

Sterols and sphingolipids are synthesized in the endoplasmic reticulum. Both of them are rare in the ER (5 mol% of lipids) but abundant in the trans-Golgi and plasma membrane (30–40 mol%) [17–19]. Although the mechanism by which sphingolipids and sterols are move up the concentration gradient into the PM is not fully understood, a possible role for cytoplasmic coat protein (COP) vesicular and non-vesicular lipid transport proteins that mediate retrograde membrane

CONTACT Fu-Cheng Lin fuchenglin@zju.edu.cn State Key Laboratory for Managing Biotic and Chemical Treats to the Quality and Safety of Agro-products, Institute of Plant Protection and Microbiology, Zhejiang Academy of Agricultural Sciences, Hangzhou, Zhejiang, China
Supplemental data for this article can be accessed online at https://doi.org/10.1080/15548627.2023.2181739

transport [19,20]. In yeast cells, *de novo* synthesized ceramide and very long acyl chain phytoceramide (C26) in the ER can be delivered to the cis-Golgi via COPII vesicles to form complex sphingolipids. However, the shorter acyl chain ceramides are most likely to be delivered to the cis-Golgi by a non-vesicular mechanism in mammalian cells [21]. In addition, some proteins are involved in sterols transport in mammals and yeast. In yeast, Osh proteins were found to regulate the organization of sterols in the PM. in temperature-conditioned yeast mutants lacking all functional Osh proteins, the bidirectional movement of sterols between the ER and PM was not affected, suggesting that other sterol transport proteins are present in yeast cells [21,22].

In recent years, the VAD1 analog of StAR-related lipid transfer (VASt) domain-containing proteins have been identified in eukaryotes. However, although these structural domains are present in all major eukaryotic lineages, they have not yet been assigned molecular functions [23]. In *Arabidopsis thaliana*, the VASt domain-containing protein VAD1 regulates programmed cell death [14,24]. The presence of a GRAM domain in VAD1 suggests that its function may require lipid binding, but the role of VAD1 at the subcellular level is currently unknown [23]. In mammals, the VASt domain-containing proteins GRAMD1A/Aster-A, GRAMD1B/Aster-B, and GRAMD1C/Aster-C bind cholesterol and facilitate its removal from the plasma membrane [15]. In *Saccharomyces cerevisiae*, there are six VASt domain-containing proteins, namely Lam1, Ysp2/Lam2, Sip3/Lam3 and Lam4 to Lam6 [16]. The deletion of a *LAM* gene alone does not affect yeast growth but increases the resistance of yeast cells to amphotericin B, a cell membrane sterol-destroying substance, suggesting that Lam-family proteins are also involved in the distribution of sterols in the cell membrane [25–28]. In addition, new findings suggested that Ysp2 and Sip3 localized at membrane contact sites, play a role in ER-PM sterol transport. Deletion of *Ysp2* or *Sip3* lead to sterol accumulation in PM and increased sensitivity to sphingolipid synthesis inhibitors myriocin [28]. However, the identification and functions of VASt domain-containing proteins have not yet been reported in plant pathogenic fungi.

Rice blast disease, caused by *Magnaporthe oryzae* (syn *Pyricularia oryzae*), is one of the most devastating diseases and poses a major challenge to global food production and security [29–31]. The infection process of *M. oryzae* is initiated by a mature appressorium produced by a three-celled conidium [32]. In the rice blast fungus *M. oryzae*, our previous studies identified two VASt domain-containing proteins and found that MoVast1 acts as a novel sterol transfer protein regulating autophagy, membrane tension, and sterol homeostasis [33]. Although MoVast2 also include a VASt domain, the functions of MoVast2 remain to be explored. In this study, we analyzed the functions of MoVast2 in *M. oryzae* and found that MoVast2 is also anchored to the membrane system and is involved in lipid homeostasis. Furthermore, we determined that MoVast2 interacted with MoVast1 and MoAtg8, and colocalized at the phagophore assembly site (PAS). Loss of *MoVAST2* resulted in mislocalization of MoVast1, reduced activity of both TORC1 and TORC2, and substantially increased autophagic flux. In addition, lipid homeostasis was disrupted in both Δ*Movast1* and Δ*Movast2* mutants. Our results revealed that MoVast2 is another autophagy regulator that combined with MoVast1 coregulates appressorium development and lipid homeostasis by mediating both TORC1 and TORC2 activity in *M. oryzae*.

Results

Identification of the MoVast2 protein in M. oryzae

Our previous studies found that the VASt-domain protein MoVast1 regulates autophagy, membrane tension, and sterol homeostasis in rice blast fungus. To further explore the precise regulatory mechanisms of the VASt domain proteins, we screened the rice blast fungus database (http://fungi.ensembl.org/Magnaporthe_oryzae/Info/Index?db=core) and identified another VASt domain protein, which we named MoVast2. To explore the potential function and evolution of the VASt domain in *M. oryzae*, we obtained the VASt profile using hidden Markov models (HMM) based on 14 VASt homolog domains from yeast to humans. The HMM signature showed that the DNDNFxxxQR motif was strongly conserved from animals to fungi, suggesting that these residues may play an essential role in protein function (Fig. S1A). Next, we analyzed the homolog of VASt domain proteins in different species including *S. cerevisiae, Homo sapiens* and *M. oryzae*. A multi-sequences alignment tree implied that the VASt domain of MoVast2 displayed more similarities to Sip3 and Lam1 of yeast (Fig. S1B, C).

To further characterize VASt domain proteins, we searched the full-length VASt domain proteins in *S. cerevisiae, H. sapiens* and *M. oryzae* using the Ensembl database. The results showed that different copies of VASt domain proteins exist in diverse species. There are six VASt domain proteins in *S. cerevisiae*, named Lam1, Ysp2, Sip3, Lam4, Lam5, and Lam6. Lam1 and Sip3 contain a BAR domain, a PH domain and a VASt domain. Ysp2, Lam4, Lam5, and Lam6 contain a GRAM domain and a VASt domain. However, Ysp2 and Lam4 contain two VASt domains. In *H. sapiens*, three VASt domain-containing proteins were identified and named GRAMD1A, GRAMD1B and GRAMD1C, all of which have a GRAM domain and a VASt domain. In contrast, only two VASt domain-containing proteins were found in *M. oryzae*. MoVast2 has an additional BAR structural domain and PH structural domain compared to MoVast1 (Fig. S1D). These results demonstrated that the VASt domain is conserved in many species and is frequently associated with lipid binding domains such as GRAM and PH, suggesting a functional link between VASt and lipid-binding domains.

MoVast2 interacts with MoVast1 and MoAtg8, and colocalized at the PAS

To explore the relationship between MoVast1 and MoVast2, we constructed the GFP-MoVast1 and MoVast2-Flag vectors and co-transferred them into the wild-type strain Guy11. The MoVast2-Flag bands were detected by immunoprecipitation in cells expressing GFP-MoVast1 but not those expressing only GFP, suggesting that MoVast1 interacts with MoVast2

in vivo (Figure 1A). The interaction of MoVast1 and MoVast2 was also validated by bimolecular fluorescence complementation (BiFC). Expression of chimeras containing MoVast2 fused to the N terminus of Venus YFP and MoVast1 fused to the YFPC terminus resulted in a fluorescent signal indicating that the split YFP halves were brought into proximity by the MoVast1-MoVast2 interaction (Figure 1B); neither construct expressed along with the MoPil1 vector resulted in a positive signal. Similarly, the DUAL split-ubiquitin system of yeast two-hybrid assays that was developed for the detection of membrane protein interactions also revealed an interaction between MoVast1 and MoVast2 based on growth on selective media plates (Figure 1C). Our previous studies found that MoVast1 can interact with MoAtg8. To examine the

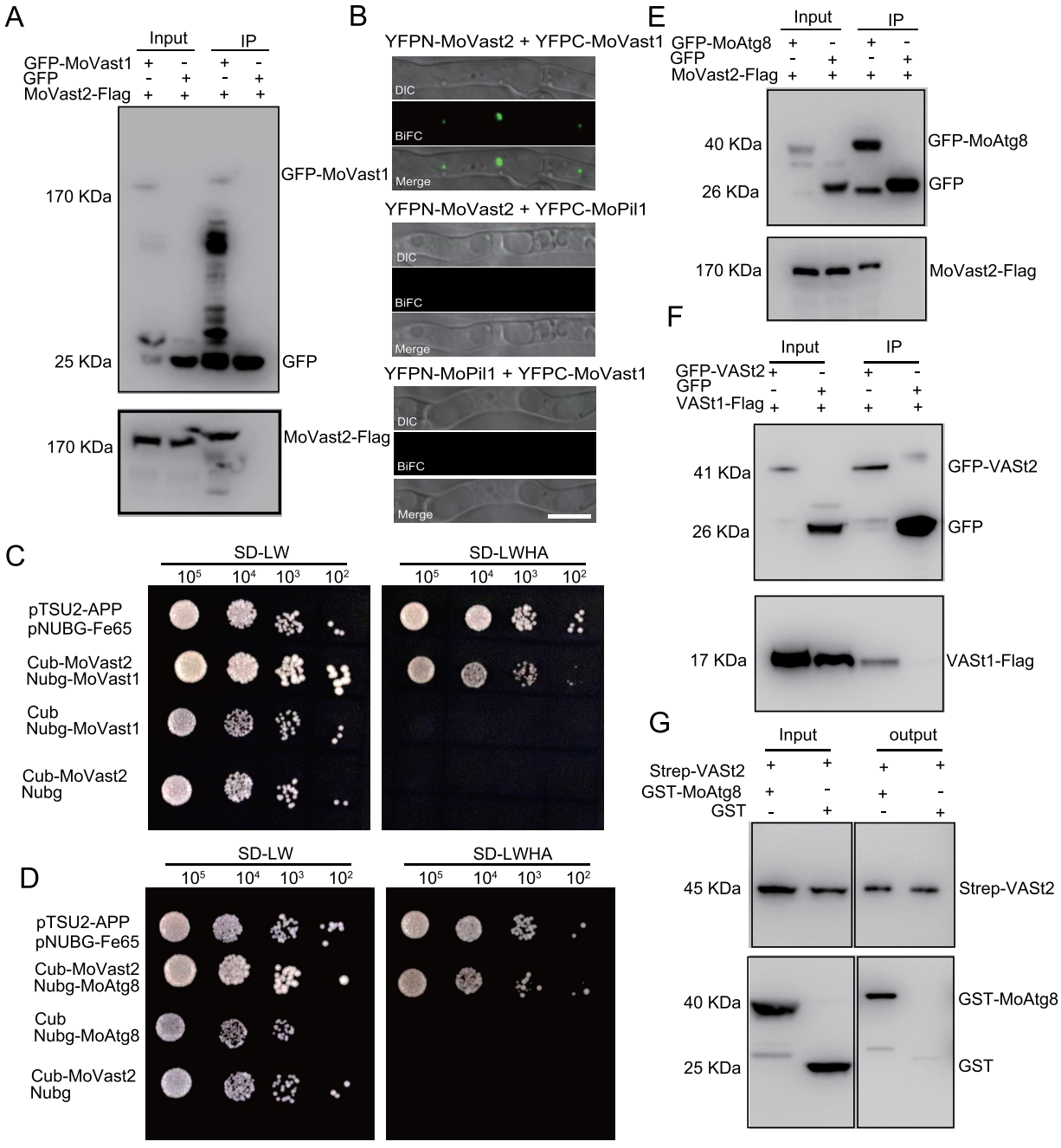

Figure 1. MoVast2 interacts with MoVast1 and MoAtg8. (A) The relationship between MoVast1 and MoVast2 was detected by co-immunoprecipitation (co-IP) assay. The MoVast2-Flag bands were detected following GFP-MoVast1 immunoprecipitation. (B) Bimolecular fluorescence complementation (BiFC) was employed to explore the interaction relationship between MoVast1 and MoVast2. The YFP signals can be observed in YFPN-MoVast2 and YFPC-MoVast2 co-transformed strains but not in YFPN-MoPil1 and YFPC-MoVast1, or YFPN-MoVast2 and YFPC-MoPil1 co-transformed stains. Bar: 10 μm. (C) The DUAL membrane system of yeast two-hybrid assay confirmed MoVast1-MoVast2 interactions. The yeast transformants with the indicated paired plasmids were diluted and cultured on the SD medium lacking leucine and tryptophan (SD-LW; selecting for transformants) and medium also lacking histidine and adenine (SD-LWHA; selecting for protein-protein interaction) for 4 days prior to imaging. pTSU2-APP with pNUBG-Fe65 was used as a positive control and Cub with Nubg-MoVast1, and Cub-MoVast2 with Nubg were used as negative controls. (D) The DUAL membrane system assay was adopted for testing the interaction between MoVast2 and MoAtg8. (E) A co-IP assay tested the interaction between MoVast2 and MoAtg8. (F) An affinity-isolation assay was adopted for examining the interaction between the VASt domains of MoVast2 (VASt2) and MoVast1 (VASt1). GFP with VASt1-Flag was used as a negative control. (G) The affinity-isolation assay was used for verifying the interaction between the VASt domain of MoVast2 (VASt2) and MoAtg8.

relationship between MoVast2 and MoAtg8, we also detected the interaction between MoVast2 and MoAtg8 using co-immunoprecipitation (co-IP) and yeast two-hybrid assay. Both co-IP and yeast two-hybrid assays confirmed the interaction between MoVast2 and MoAtg8 (Figure 1D, E), indicating that MoVast2 could interact with MoVast1 and MoAtg8.

As shown in Fig. S1C, MoVast1 contains a GRAM domain and a VASt domain whereas MoVast2 contains BAR, PH and VASt domains. To determine whether the VASt domain of MoVast2 is required for the interaction between MoVast1 and MoAtg8, we expressed the VASt domain of MoVast1and MoVast2, and full-length MoAtg8 using *Escherichia coli* DE3 cells. The affinity-isolation assay showed that the VASt domain of MoVast2 interacted with both the VASt domain of MoVast1 and MoAtg8, indicating the VASt domain has a role in maintaining the relationship between MoVast1, MoVast2 and MoAtg8 (Figure 1F, G).

To explore the interaction sites of MoVast2 with MoVast1 and MoAtg8, we used three markers, RFP-MoAtg17, RFP-MoAtg18 and RFP-MoPil1 to identify where MoVast2-MoVast1 and MoVast2-MoAtg8 interacted. The autophagy protein Atg17 has been reported to localize to the PAS, which is thought to be the organizing center for the formation of the sequestering vesicles, autophagosomes and Cvt vesicles that form during bulk and specific autophagy [34]. In humans, Atg18 was reported to deliver some phospholipids, such as phsophatidylinositol-3-phosphate to the PAS and functions as a novel PtdIns3P scaffold at the onset of autophagy. In addition, the Atg18 protein accumulates at the phagophore to form puncta structure, which is suitable to analyze levels of phagophore formation and thus assess mammalian autophagy [35,36]. In yeast, Pil1 is a core eisosome protein, coordinates regulation of TORC2 signaling at MCC (membrane compartment occupied by Can1) domain [37]. In *M. oryzae*, we transferred the RFP-MoAtg17, RFP-MoAtg18, and RFP-MoPil1 to MoVast2-MoVast1 and MoVast2-MoAtg8 interaction strains, respectively. Interestingly, both the MoVast2-MoVast1 and MoVast2-MoAtg8 colocalized with MoAtg17 in *M. oryzae* (Figure 2A). In addition, the RFP-MoAtg18 formed puncta structures localized around the vacuole and partially colocalized with both the MoVast2-MoVast1 and MoVast2-MoAtg8 (Figure 2B). However, colocalizations were not found in MoVast2-MoVast1 or MoVast2-MoAtg8 strains that co-expressed RFP-MoPil1 (Figure 2C). These results suggested that MoVast2 interacted with MoVast1 and MoAtg8 at the PAS, but not at the MCC domain.

Structure of the VASt2, VASt2-MoAtg8 and VASt2-VASt1 complex in M. oryzae

To better understand the structure of VASt2 and the interaction surface between VASt2, VASt1 and MoAtg8, we constructed the three-dimensional (3D) structures of VASt2, VASt1, VASt2-MoAtg8 and VASt2-VASt1 complexes using AlphaFold2, which is a recently developed protein predictive platform based on a machine learning method with high accuracy [38]. In the VASt2 model, there are six β sheets, three α helices and two Ω loops constructed by AlphaFold2 with a pLDDT of 86.1. Following this, we also constructed the VASt1 model and found a pLDDT of 94.3 for VASt1, which has a similar structure to VASt2, although the sequence similarity in the secondary structure is not high (Figure 3A-C). Our previous studies found that VASt2 can interact with VASt1 and MoAtg8. To further confirm the interaction surface, we predicted the VASt2-VASt1 and VASt2-MoAtg8 complexes using ColabFold based on AlphaFold2. The interaction surface of VASt2-VASt1 and VASt2-MoAtg8 complex are displayed in Figure 3D and Figure 3E. In Figure 3D, the Ω loop areas of VASt2 had a contact surface with the α3 helix and the Ω loop areas of VASt1. In the VASt2-MoAtg8 complex, the β sheets of VASt2 were in contact with the Ω loop areas and the N terminus of MoAtg8. These results suggest that there is a difference in the interaction surface between VASt1 and MoAtg8.

MoVast2 is involved in the development and virulence of M. oryzae

To further confirm the function of MoVast2, we deleted the corresponding gene using a homologous recombination strategy and successfully obtained Δ*Movast2*, which was verified by southern blot (Fig. S2). A plasmid encoding *GFP-MoVAST2* was transformed into the Δ*Movast2* null mutant to generate the complemented wild-type control strain (*ΔMovast2-C*). The Δ*Movast2* strain showed slightly slower growth compared with the wild-type Guy11 strain at 25°C (Figure 4Ai). The Δ*Movast2* mutant had reduced conidial production and altered conidial morphology, with most conidia being short and curved (Figure 4Aii-iii, B-D).

The appressoria of *M. oryzae* plays a vital role in virulence by providing sufficient enough penetration turgor to infect their host [31]. To examine whether MoVast2regulates the development of appressoria in *M. oryzae*, we induced the appressoria on an artificial inductive surface and observed their morphology by microscopy. In the wild-type Guy11 strain and the complemented *ΔMovast2-C* strain, nearly 80% of the appressoria were formed at 6 h post-inoculation (hpi), compared to 25% in Δ*Movast2* (Figure 5A, B). Less than 50% of melanized appressoria could develop in the Movast2 mutant at 12 h. In contrast, the Guy11 strain had melanized appressorium rates of over 80% at 12 h (Figure 5C). Next, we tested the pathogenicity of Δ*Movast2* on rice leaves using conidia. As expected, the disease lesions were smaller in the Δ*Movast2* mutant than in the wild-type Guy11 and complemented strains (Figure 5D-F). Finally, we studied the leaf sheath infection conditions at 24, 48 and 72 hpi to further explore the infection progression in the Δ*Movast2* mutant. At 24 hpi, the appressoria were formed and the invasive hyphae (IH) could infect the first cell of rice in the wild-type strain and the complemented strain, whereas almost no IH were found in Δ*Movast2*, although the appressoria had already formed. At 48 and 72 hpi, with the wild-type strains nearly 80% of infection structures were formed and these had expanded to the neighboring cells. However, with Δ*Movast2*, only about 60% of the infected structures could be found, and this 40% was still limited to the initially infected cells at 48 hpi. Even at 72 hpi, only 20% of the cells could be

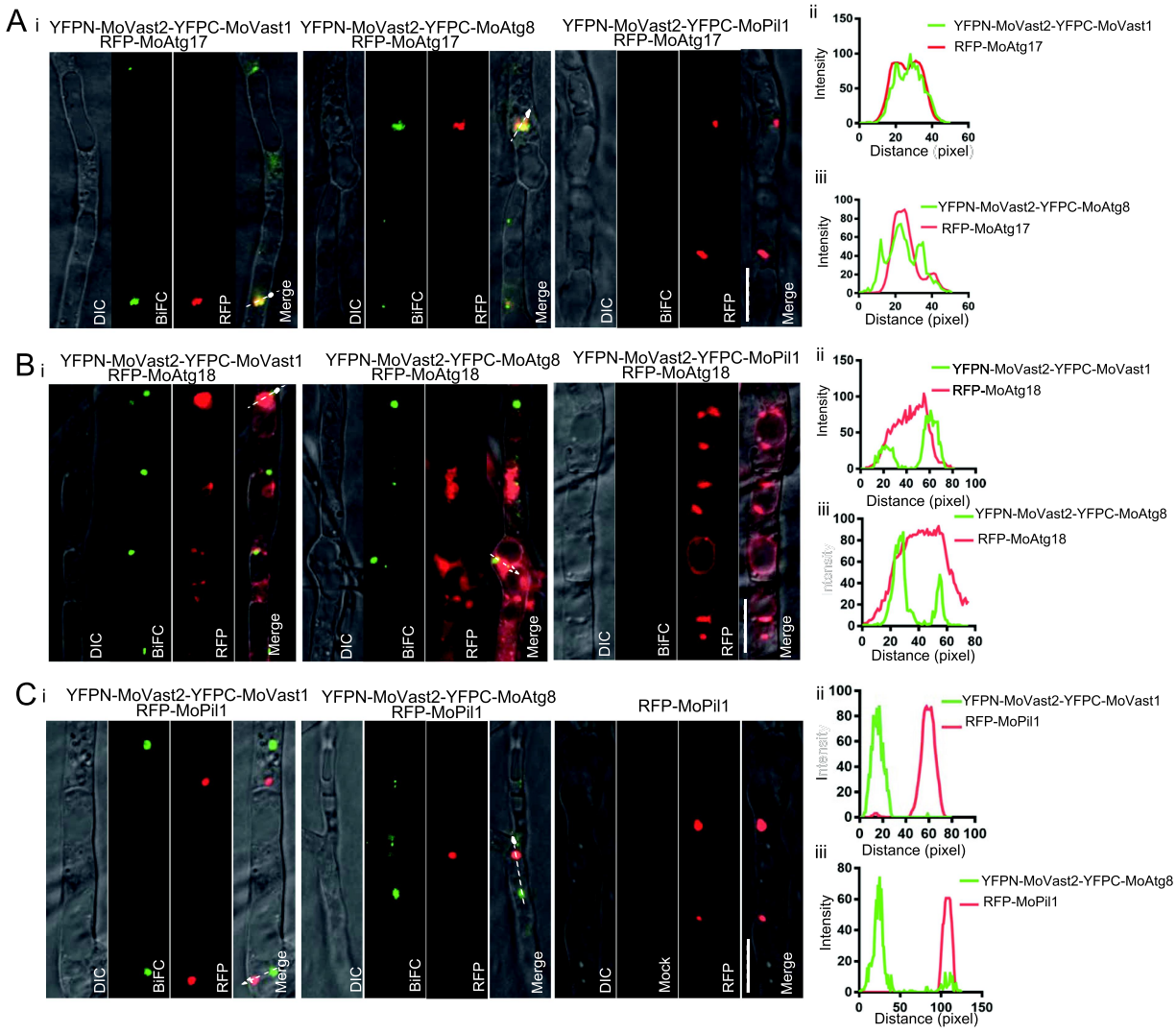

Figure 2. Colocalization of MoVast2-MoVast1 and MoVast2-MoAtg8 in PAS. (Ai)The localization of MoVast2-MoVast1, MoVast2-MoAtg8, and RFP-MoAtg17 were observed by confocal microscopy. Bar: 10 μm. (Aii & Aiii) Fluorescence densities of MoVast2-MoVast1, MoVast2-MoAtg8, and RFP-MoAtg17 were analyzed using ImageJ software. (Bi) The localizations of MoVast2-MoVast1, MoVast2-MoAtg8, and RFP-MoAtg18 were observed by confocal microscopy. Bar: 10 μm. (Bii & Biii) Fluorescence densities of MoVast2-MoVast1, MoVast2-MoAtg8, and RFP-MoAtg18 were analyzed. (Ci) The localizations of MoVast2-MoVast1, MoVast2-MoAtg8, and RFP-MoPil1 were observed. Bar: 10 μm. (Cii & Ciii) Fluorescence densities of MoVast2-MoVast1, MoVast2-MoAtg8, and RFP-MoPil1 were analyzed.

expanded beyond two (Figure 5G, H). These results demonstrated that MoVast2 plays a role in appressoria development and virulence in *M. oryzae*.

MoVast2 responds to rapamycin and regulates autophagy

Our previous studies confirmed that MoVast1 negatively regulated TOR activity. In this study, we tested the role of MoVast2 in TOR regulation. When treated with rapamycin (a TOR kinase inhibitor) on CM medium at 25°C for 7 days, the Δ*Movast2* mutant displayed stronger growth defects compared with the wild-type strains and the complemented Δ*Movast2-C* strain (Figure 6A, B). In yeast and animals, TORC1 acts as an upstream regulator that controls the autophagic process by phosphorylating the autophagic proteins Atg13 and Atg1, inhibiting their function [39]. To test whether MoVast2 affects TORC1 activity, we assayed the activity of TORC1 by the phosphorylation level of MoRps6, which is a reliable marker to measure TORC1 activity [40,41]. Immunoblotting assay found that the phosphorylation level of MoRps6 was significantly reduced when treated with rapamycin for 3 h and was restored at 6 hpi. However, in the Δ*Movast2* mutant, the band of p-MoRps6 was weaker compared with the wild-type under CM conditions and drastically dropped after 3 h treatment with 100 ng/ml rapamycin and did not recover at 6 hpi (Figure 6C). These results indicated that the activity of TORC1 was impaired in the Δ*Movast2* mutant. To further explore the autophagy process, a plasmid expressing GFP-MoAtg8 was transformed into the wild-type and the Δ*Movast2* mutant by *in situ* methods [42]. GFP puncta developed when the mycelium was cultivated in CM media for two days, and neither the wild-type nor the Δ*Movast2* mutant strain showed any appreciable differences (Figure 6D, E). However, a part of GFP signaling was discovered in vacuoles in Δ*Movast2* mutant, but not in the wild-type strain (Figure 6G). The GFP puncta were diminished in both strains following autophagy induction in SD-N medium

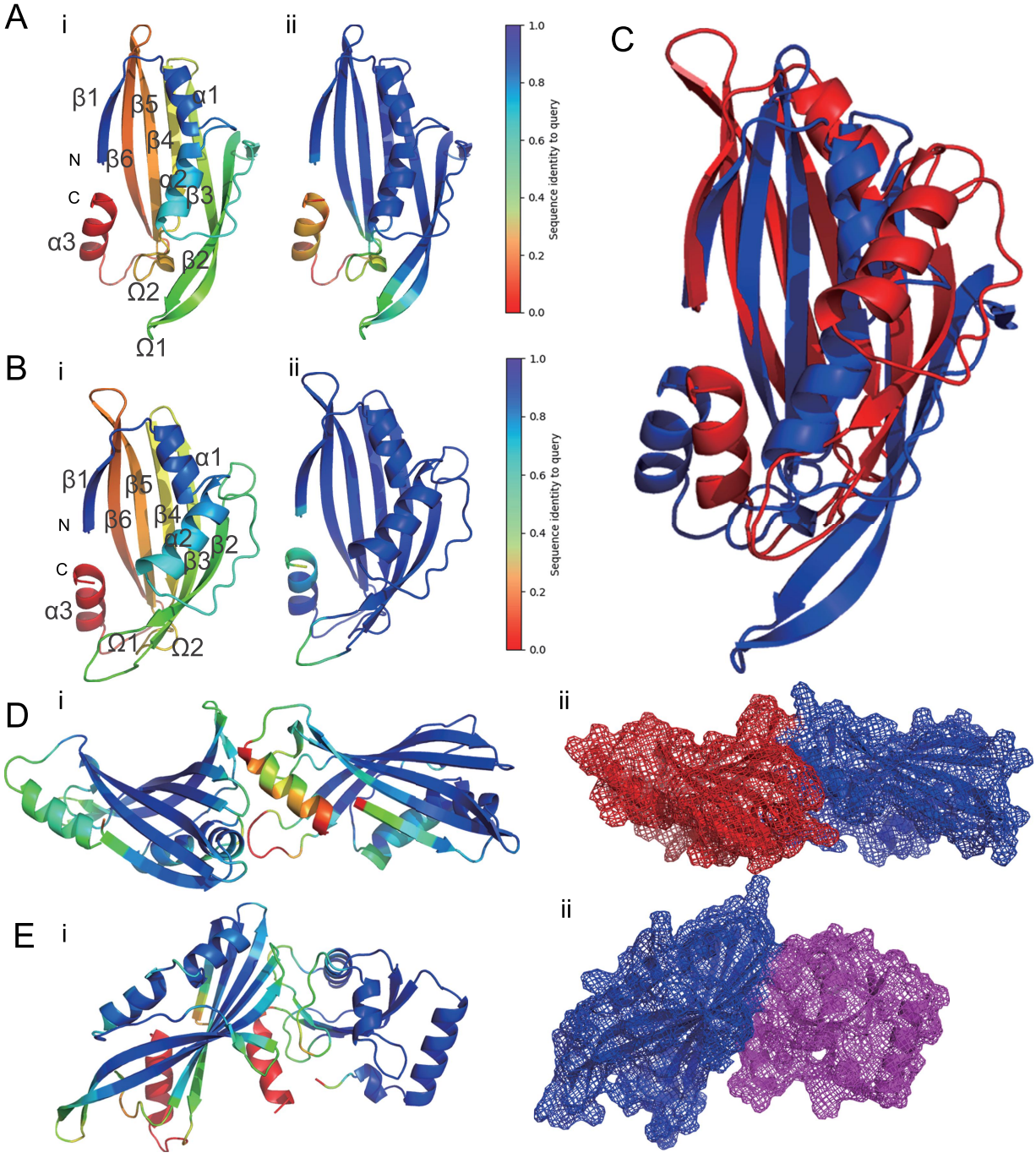

Figure 3. Structures of the VASt2, VASt2-MoAtg8 and VASt2-VASt1 complexes in *M. oryzae*. (A) 3D structure of the VASt domain of MoVast2. (Ai) The structure was constructed using ColabFold based on AlphaFold2. (Aii) Structure confidence of the VASt domain of MoVast2 by the colored polymers based on pLDDT (score = 86.1). (Bi) 3D structure of VASt domain of MoVast1. (Bii) structure confidence of the VASt domain of MoVast1 by the colored polymers based on pLDDT (score = 94.3). (C) The alignment structures of VASt1 in blue and VASt2 in red. (D) Predicted structure of the VASt2-VASt1 complex. (Di) Cartoon model of the VASt2-VASt1 complex. (Dii) Mesh model constructed by PyMOL software. (E) Predicted structure of the VASt2-MoAtg8 complex. (Ei) The cartoon model; (Eii) the mesh model.

for 4 h; while fewer GFP puncta were found in the Δ*Movast2* mutant (Figure 6D).

To further confirm how MoVast2 regulates autophagy flux at the molecular level, we evaluated the content of GFP-MoAtg8 and free GFP using western blot. In this assay, a population of GFP-MoAtg8 is delivered to the vacuole inside autophagosomes; the MoAtg8 portion of the chimera is degraded, whereas GFP is relatively stable and can be monitored to reflect the level of autophagic flux. In the wild-type Guy11 strain, the basal level of autophagy was very low with almost no detectable free GFP at time zero. When induced for 4 h in SD-N medium, the free GFP band increased concomitant with a decrease in the full-length chimera. In contrast, there was a much higher level of free GFP starting at time zero in the Δ*Movast2* mutant, indicating an elevated basal autophagy activity. In both strains there was an increase in GFP-MoAtg8 or free GFP following autophagy induction, which corresponds to the increased expression of MoAtg8 under these conditions; however, the increase in the Δ*Movast2* mutant was substantially greater than that seen with the wild-type strain (Figure 6F).

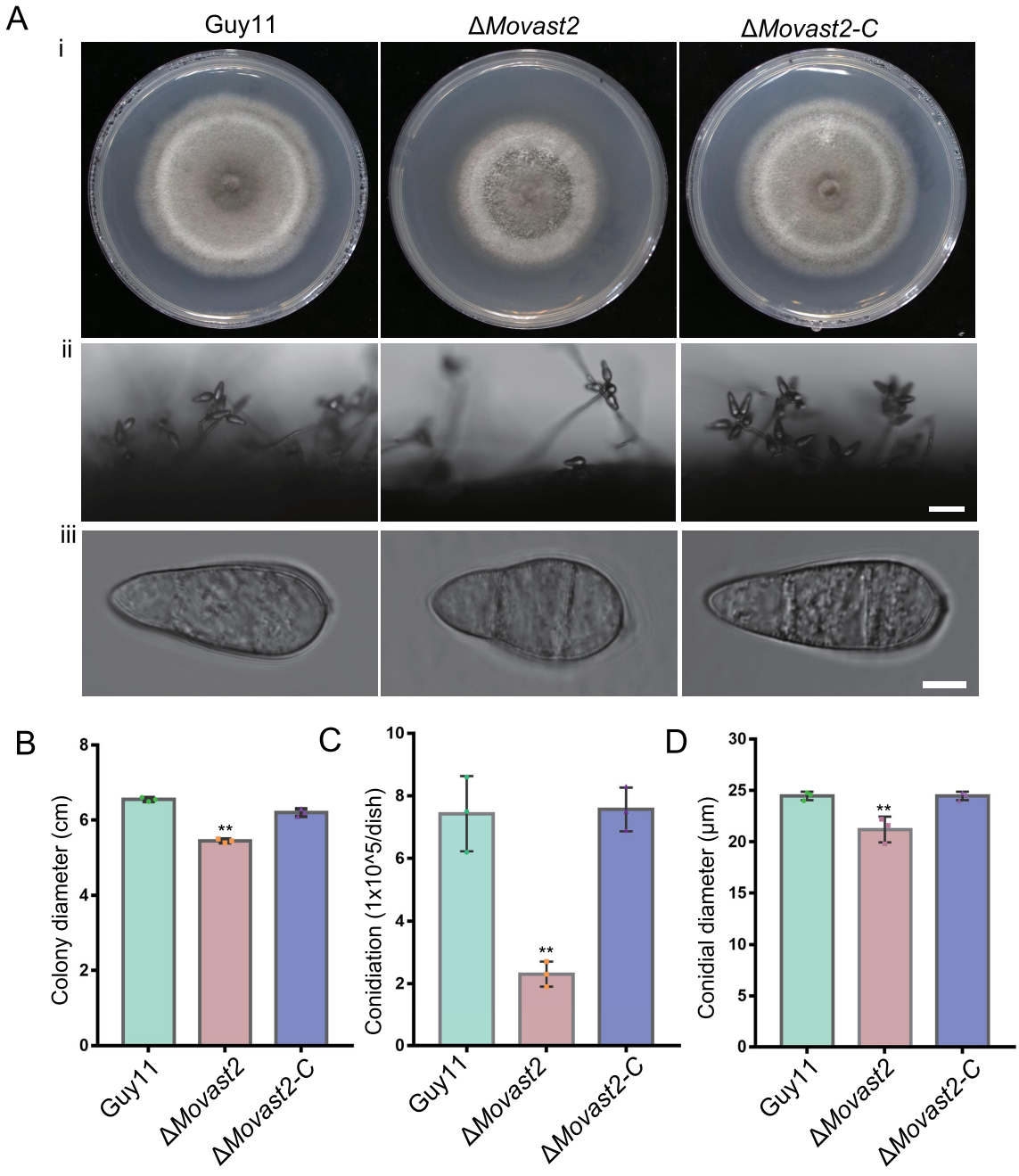

Figure 4. MoVast2 is involved in conidia development. (A) All strains were cultured on CM medium for 7 days at 25°C with a light-dark time of 16 h-8 h and were observed for (I) morphology, (ii) conidia and conidiophores, and (iii) morphology of conidia. Bar: 50 μm in Aii and 5 μm in Aiii. Δ*Movast2-C*, the complemented null strain. (B, C, D) The colony diameter, conidia and conidial diameter were calculated and analyzed using Prism 7.0 software. Asterisks represent statistically significant differences (** $p < 0.01$).

Conidial autophagy was recently discovered to be essential for *M. oryzae's* pathogenicity [33]. To examine the role of MoVast2 in conidial autophagy progression, the autophagy flux in conidia was measured. In the Δ*Movast2* mutant, the melanized appressorium formed after the conidia were induced for 12 h, during which time the majority of autophagosomes were destroyed in the conidium and new autophagosomes were produced in the appressorium. However, few green fluorescent dots were found in either conidia or appressoria at 12 h compared with the wild-type Guy11 strain (Figure 6H, I). These findings demonstrated that *MoVAST2* deletion compromises the TOR activation and triggers an inappropriate autophagy pathway.

MoVast2 is involved in lipid homeostasis

Sip3, a protein that is homologous to MoVast2 *in S. cerevisiae*, is involved in the response to numerous environmental stresses and is sensitive to lipid synthesis inhibitors[26][]. To explore the roles of MoVast2 in *M. oryzae*, we exposed the Δ*Movast2* strain to azoles and some lipid synthesis inhibitors. The Δ*Movast2* strain showed resistance to these azoles when treated with 1 μg/ml triazolone, 0.25 μg/ml terbinafine, 0.25 μg/ml tebuconazole, 0.5 μg/ml prochloraz, and 0.25 μg/ml tebuconazole, which are broad-spectrum fungicides that suppress ergosterol production. Amphotericin B, which

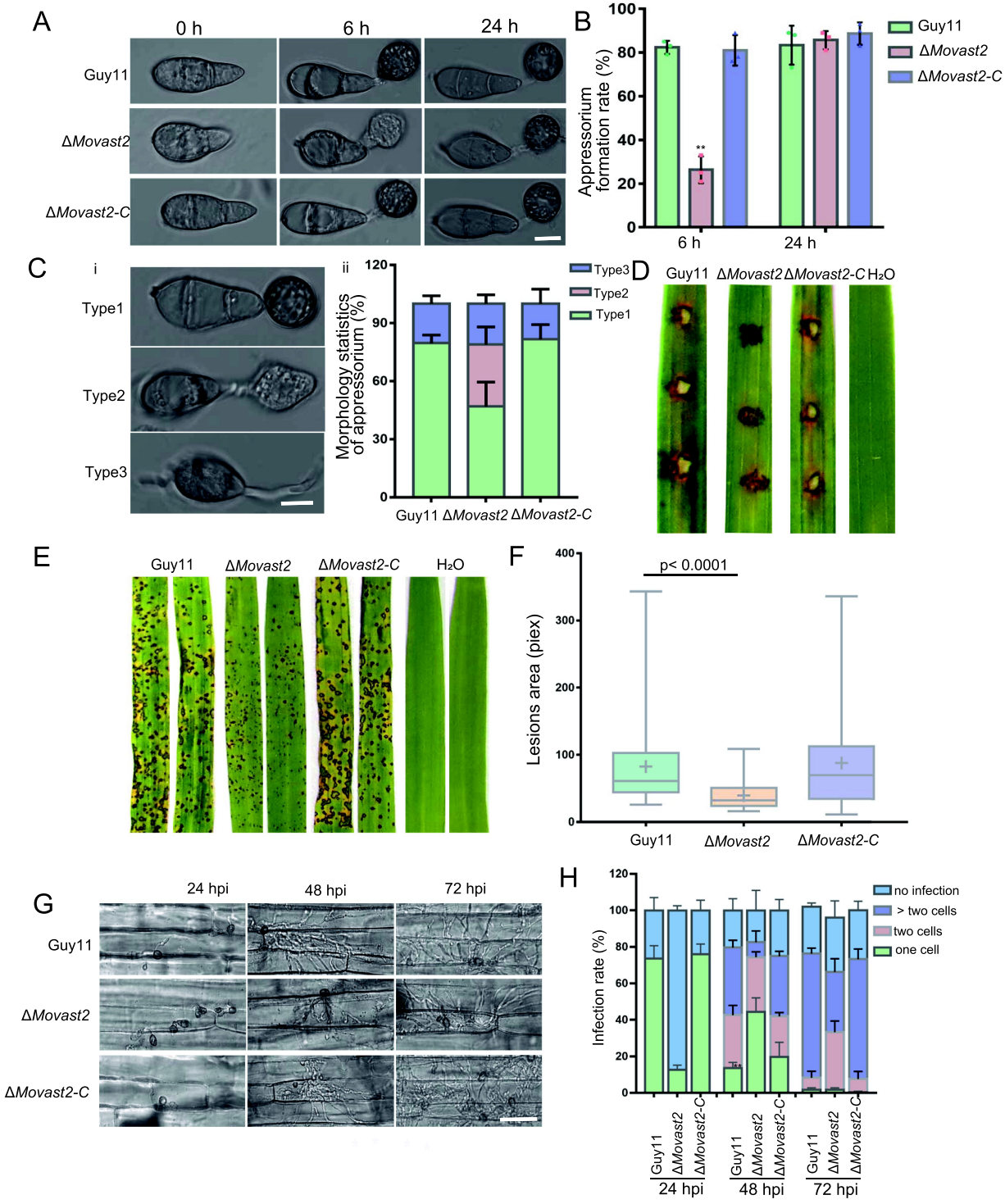

Figure 5. MoVast2 regulates appressoria development and virulence in *M. oryzae*. (A) Observation of appressorium morphology of Guy11, Δ*Movast2*, and the complemented strain. The conidia of the indicated strains were collected and diluted at 10^5 conidia/ml and dropped onto a hydrophobic plastic coverslip at 22°C for 0 h, 6 h and 24 h, then observed using a microscope. Bar: 10 μm. (B) The appressorium formation rate was counted using Prism 7.0 and analyzed using a t-test; asterisks represent statistically significant differences (** $p < 0.01$). (C) The morphology statistics of appressoria in Guy11, Δ*Movast2*, and the complemented strain at 12 hpi. Type 1 corresponds to the normal type with melanized appressorium; type 2 represents abnormal appressoria without melanization; and type 3 indicates no appressorium. Bar: 10 μm. (D) The disease lesions were tested in cut rice leaves using 1×10^5 spores/ml conidia of Guy11, Δ*Movast2*, and the complemented strain. (E) The conidia infection assay was used for testing the virulence in rice seedlings. (F) The lesion areas were counted and calculated using ImageJ and Prism 7.0 software. (G) The sheaths incubation assay was employed for detecting the infection conditions of the indicated strains. Asterisks mark invasive hyphae. Bar: 50 μm. (H) The infection rate was quantified and statistically analyzed using Prism 7.0 software.

disrupts the PM by attaching to ergosterols, however, reduced growth of the Δ*Movast2* strain (Fig. S3A, B). These results indicated that sterols biosynthesis was disrupted. Then, we detected the content of sterols of the PM using filipin stain as described by Zhu et al [33]. In the Δ*Movast2* strain, the filipin signal was significantly higher than the wild-type Guy11 and

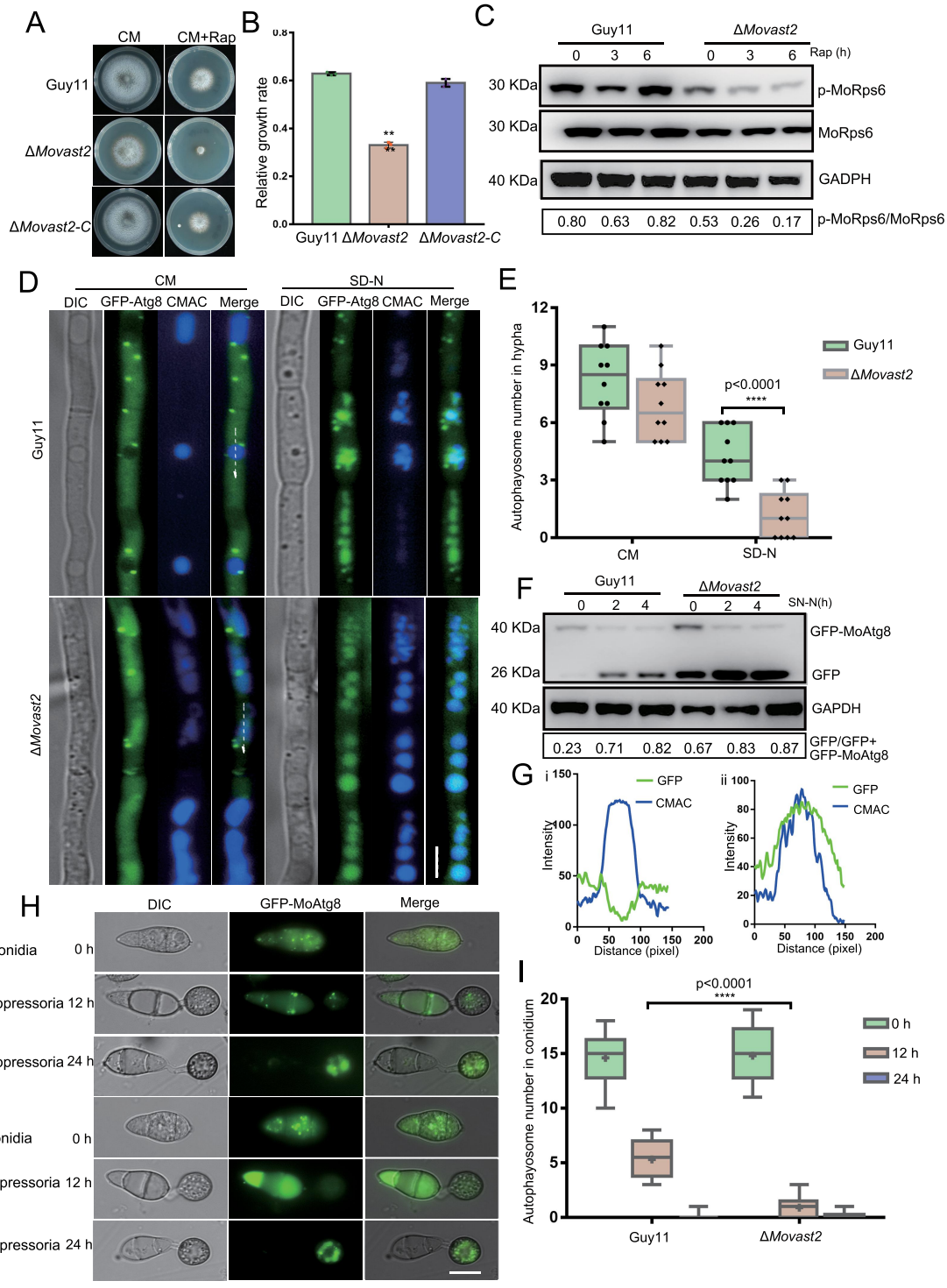

Figure 6. MoVast2 responds to rapamycin and regulates autophagy. (A) The growth conditions of Guy11, Δ*Movast2*, and the complemented strain in CM medium and CM medium with 100 ng/ml rapamycin. (B) The relative growth rate was measured and analyzed with Prism 7.0. Asterisks represent statistically significant differences (** $p < 0.01$). (C) Western blot analysis of the phosphorylation of MoRps6 in the wild-type strain and Δ*Movast2* mutant. The mycelia were cultured in CM medium for 2 days followed by induction with 100 ng/ml rapamycin for 3 and 6 h. Proteins were extracted with TCA-acetone-SDS and the phosphorylation of MoRps6 were measured using MoRps6 and p-MoRps6 antibody. (D) The autophagy level was evaluated using GFP-MoAtg8. The Guy11 and Δ*Movast2* strains were marked with GFP-MoAtg8 and cultured in CM medium for 2 days and then transferred to SD-N medium for 4 h. Mycelia were stained with CMAC and observed by fluorescence microscopy with a GFP laser and UV laser. Bar: 10 μm. (E) Autophagosomes were counted in the Guy11 and Δ*Movast2* strains. The data were calculated using Prism 7.0. (F) The autophagy flux was monitored with the GFP-MoAtg8 degradation processing assay. (G) Fluorescence densities of GFP-MoAtg8 and CMAC in Guy11 and Δ*Movast2* mycelium vacuoles at CM condition were measured using ImageJ software. (H) The autophagy flux was observed in conidia and appressorium in cells expressing GFP-MoAtg8. Bar: 10 μm. (I) The autophagosomes of Guy11 and Δ*Movast2* were counted in conidia. Data were calculated using Prism 7.0.

the Δ*Movast2-C* strain, which indicated that the PM sterols were significantly higher in the Δ*Movast2* strain than that in the Guy11 and Δ*Movast2-C* strains, implying that loss of MoVast2 led to accumulation of sterol content to increase the resistance to azoles (Fig. S3C, 3D). In addition, the cell membrane permeability was also increased in Δ*Movast2* (Fig.

S3E-G), indicating the content of sterols in the PM would affect cell membrane permeability.

Sterols and sphingolipids are two key factors to maintain PM homeostasis. We are interested in finding out if changing the sterol content can have an impact on sphingolipids. Accordingly, we further detected the changes of sphingolipids in the wild-type strain, the Δ*Movast2* mutant, and the Δ*Movast2-C* strain. Surprisingly, the Δ*Movast2* strain was highly sensitive to myriocin, which is a sphingolipid synthesis inhibitor that binds to serine palmitoyltransferase (Spt1) and inhibits its activity (Figure 7(A and B)). When the Δ*Movast2* strain was exposed to 2 μM myriocin, at which concentration appressoria could still develop; however, the mutant showed very little pathogenic potential compared to Guy11 and the Δ*Movast2*-C strains (Figure 7C). These results suggested that loss of MoVast2 leads to accumulation of sterol content on PM, thereby inhibiting sphingolipid synthesis. As shown in Figure3A, Δ*Movast2* strain displayed higher resistance to sterols synthesis inhibitors. We wonder if inhibition of sterol synthesis would affect sphingolipid homeostasis. Therefore, we added both 1 μg/ml triazolone and 2 μM myriocin to CM medium and added the same concentration DMSO to CM medium as a control. After 7 days of culture, we were surprised to find that the Δ*Movast2* strain was loss sensitive to myriocin when treated with 1 μg/ml triazolone compared with the wild type (Figure 7D, E), suggesting that a decrease in sterol content increases Spt1 activity. However, the reduction in the content of PM sterol by triazolone could not increase the activity of Spt1 in the wild-type strain (Figure 7D). These results indicated that activity of MoVast2 plays crucial roles in lipid homeostasis and deletion of *MoVAST2* causes sterols reflux blockage, thereby decreasing the activity of Spt1.

To further confirm the role of MoVast2 in lipid homeostasis, we evaluated the lipids contents explored by lipidomic analyses. The list of lipids quantified in this experiment was shown in the Data Sheet S1, of which 768 lipids were quantified and 88 lipids showed a significant difference between wild-type and Δ*Movast2* (fold change > 1.5, BH adjusted p value < 0.05) (Figure 8A). Pathway enrichment analysis of KEGG showed that the dysregulated lipids such as PE, sterols, TAG, Cer and PI are involved in lipid metabolism, autophagy, fatty acid metabolism and steroid biosynthesis among other processes (Figure 8B). We mainly focused on the lipid classes of sphingolipids and sterols and found that sphingolipids Cer(d18:0/18:0), Cer(t18:0/22:0), Cer (d18:2/16:0), and Cer(d18:1/16:0) were significantly reduced in Δ*movast2*. However, the phospholipids PE(18:0/16:0), PE(14:0/18:1), PE(18:1/16:1), PE(O-16:0/18:2), PE(O-16:0/18:3), and sterol lipids ergosterol, 4α-carboxy-zymosterol, 9(11)-DHEP, and strophasterol e/f were significantly elevated in Δ*Movast2* compared to the wild type (Figure 8C-E). These results further confirmed that the loss of MoVast2 dysreguated lipid homeostasis and autophagy.

Both TORC1 and TORC2 are compromised in the ΔMovast2 *strain*

The TORC2 complex controls sphingolipid biosynthesis in yeast and mammalian cells. The AGC kinase Ypk1 is downstream of TORC2 and phosphorylates Orm1 and Orm2, and Lac1 and Lag1 to promote ceramide biosynthesis and thereby synthesize complex sphingolipids [43,44]. In yeast, the T662 site of Ypk1 was directly phosphorylated by TORC2, and thus the level of Ypk1 phosphorylation at T662 was used to monitor TORC2 activity [45]. In *M. oryzae*, the S619 site of MoYpk1 was conserved with yeast T662 and confirmed to be phosphorylated by TORC2 [33]. Thus, we used a western blot to determine the degree of MoYpk1 phosphorylation to corroborate the association between TORC2 and MoVast2. We found that the phosphorylation level of MoYpk1 was lower in the Δ*Movast2* mutant than in the wild type. Then, we continued to monitor the activity of TORC2 after treating cells with 2 μM myriocin for 2 and 4 h in CM medium. However, the phosphorylation level of MoYpk1 was still decreased compared with the wild type (Figure 9A). We thus hypothesized that MoVast2 acts as an upstream regulator to modulate TORC2.

The Δ*Movast2* strain was sensitive to rapamycin (Figure 6A), indicating the activity of TORC1 was disturbed. Therefore, we also detected TORC1 activity by the phosphorylation level of MoRps6. The phosphorylation level of MoRps6 was still lower when cells were treated with 2 μM myriocin for 2 and 4 h in the Δ*Movast2* mutant (Figure 9B), indicating that MoVast2 regulates both TORC1 and TORC2. We examined the activity of TORC1 and TORC2 in response to rapamycin therapy to understand the connection between TORC1 and TORC2. Both in the Δ*Movast2* strain and Guy11, the phosphorylated bands of p-MoRps6 significantly diminished after 100 ng/ml rapamycin was administered for 2 and 4 h. However, the phosphorylated bands of p-MoYpk1 had no significant change in the Δ*Movast2* and Guy11 strains (Figure 9C, D), indicating that TORC2 acts as an upstream regulator of TORC1 and was independent of TORC1.

The high osmolarity glycerol (HOG) pathway constitutes an obvious candidate to couple osmotic stress to TORC2 in *S. cerevisiae* [45–47]. Our previous studies demonstrated that MoVast1 is involved in hyperosmotic stress [33]. In *M. oryzae*, MoOsm1 (a homolog to yeast Hog1) kinase governs adaptive responses to host-derived ROS and is essential for the organism during hyperosmotic stress [48]. We cultured the wild-type, Δ*Movast2*, and the complemented strain *ΔMovast2-C* strains on CM medium with 1 M sorbitol for 7 days at 25°C to determine if Δ*Movast2* responds to hyperosmotic stress by controlling the phosphorylation of MoOsm1. The relative growth rate was significantly reduced compared with the complemented strain Δ*Movast2-C* (Figure 9E, F). In the wild-type Guy11 strain, the phosphorylation level of MoOsm1 (p-MoOsm1) was found by immunoblotting to have rapidly elevated after 20 min of induction and progressively decreased after 120 min. However, the p-MoOsm1 was maintained at a high level from 20 min to 120 min after hyperosmotic stress in the Δ*Movast2* strain (Figure 9G). To understand the function of TORC2 in the reaction to hyperosmotic stress we examined the level of MoYpk1. MoYpk1 showed decreased phosphorylation after being exposed to 1 M sorbitol for 20, 40 and 60 min; with a partial restoration at 120 min in the Guy11 strain. However, the p-MoYpk1 bands were very weak in the Δ*Movast2* mutant

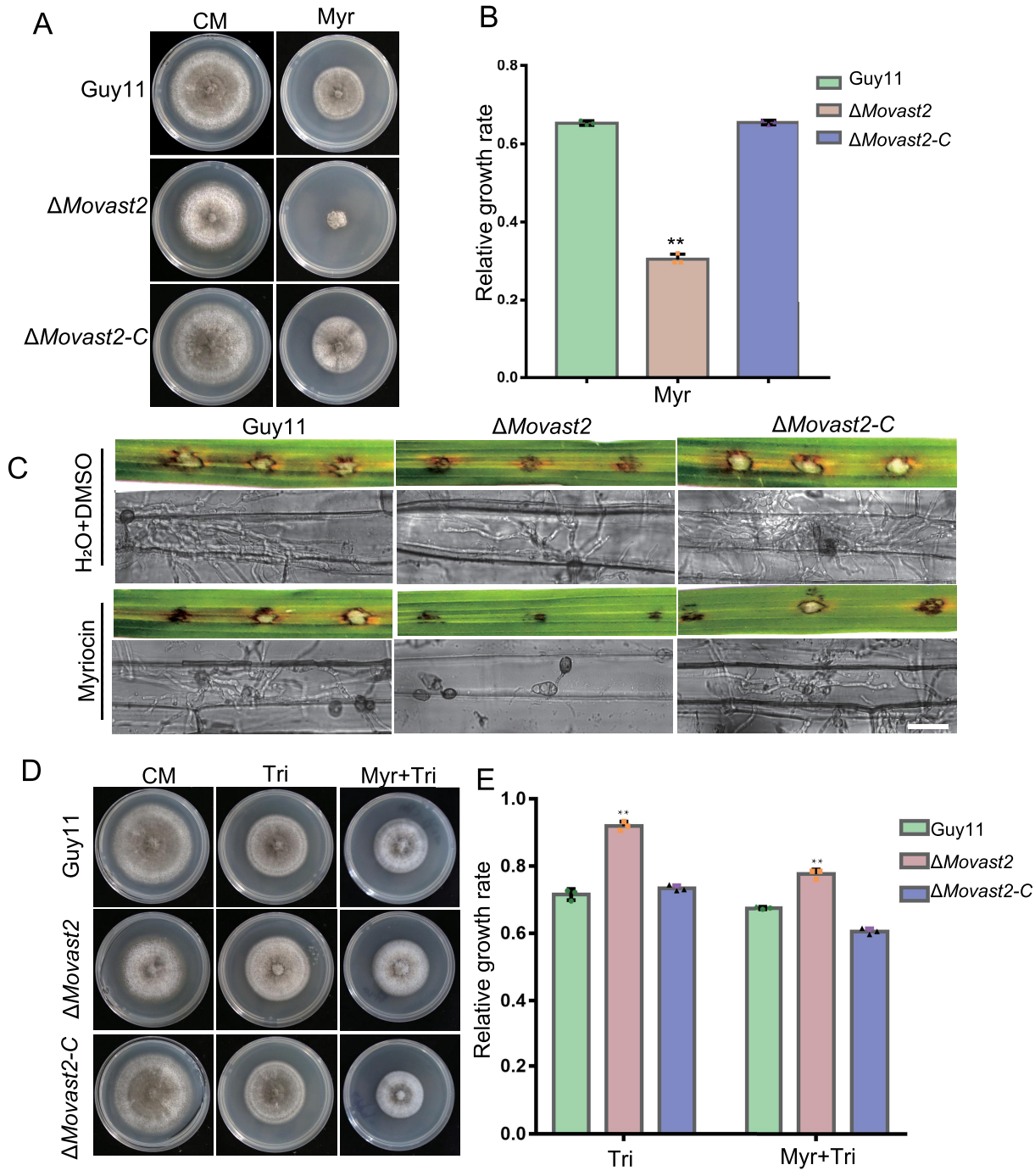

Figure 7. MoVast2 is involved in lipid homeostasis. (A) The wild-type Guy11, Δ*Movast2*, and complemented strains in CM medium and CM medium with 2 μM myriocin. (B) The relative growth rate of the indicated strains. Data were analyzed using Prism 7.0, Asterisks indicated statistically significant differences (** $p < 0.01$). (C) The disease lesions were tested on cut barley leaves with 2 μM myriocin. The sheath infection was observed using a microscope when treated with 2 μM myriocin. Bar: 50 μm. (D) The wild-type Guy11, Δ*Movast2*, and complemented strains in CM medium and CM medium with 1 μg/ml Triadimefon and 1 ug/ml Triadimefon mixed with 2 μM myriocin. (E) The relative growth rate of the indicated strains. Data were analyzed using Prism 7.0, and asterisks indicated statistically significant differences (** $p < 0.01$).

(Figure 9H). These findings showed that the activity of TORC2 decreased both in wild-type Guy11 and Δ*Movast2* under hyperosmotic stress. However, the phosphorylation of MoOsm1 steadily increased in the Δ*Movast2* strain, suggesting that the osmo-sensor(s) upstream of TORC2 may be regulated by MoVast2.

The localization of MoVast1 is disturbed in the ΔMovast2 mutant

Both MoVast2 and MoVast1 contain the VASt domain and have a similar role in appressoria formation, lipid homeostasis and autophagy. Therefore, we were interested in learning if

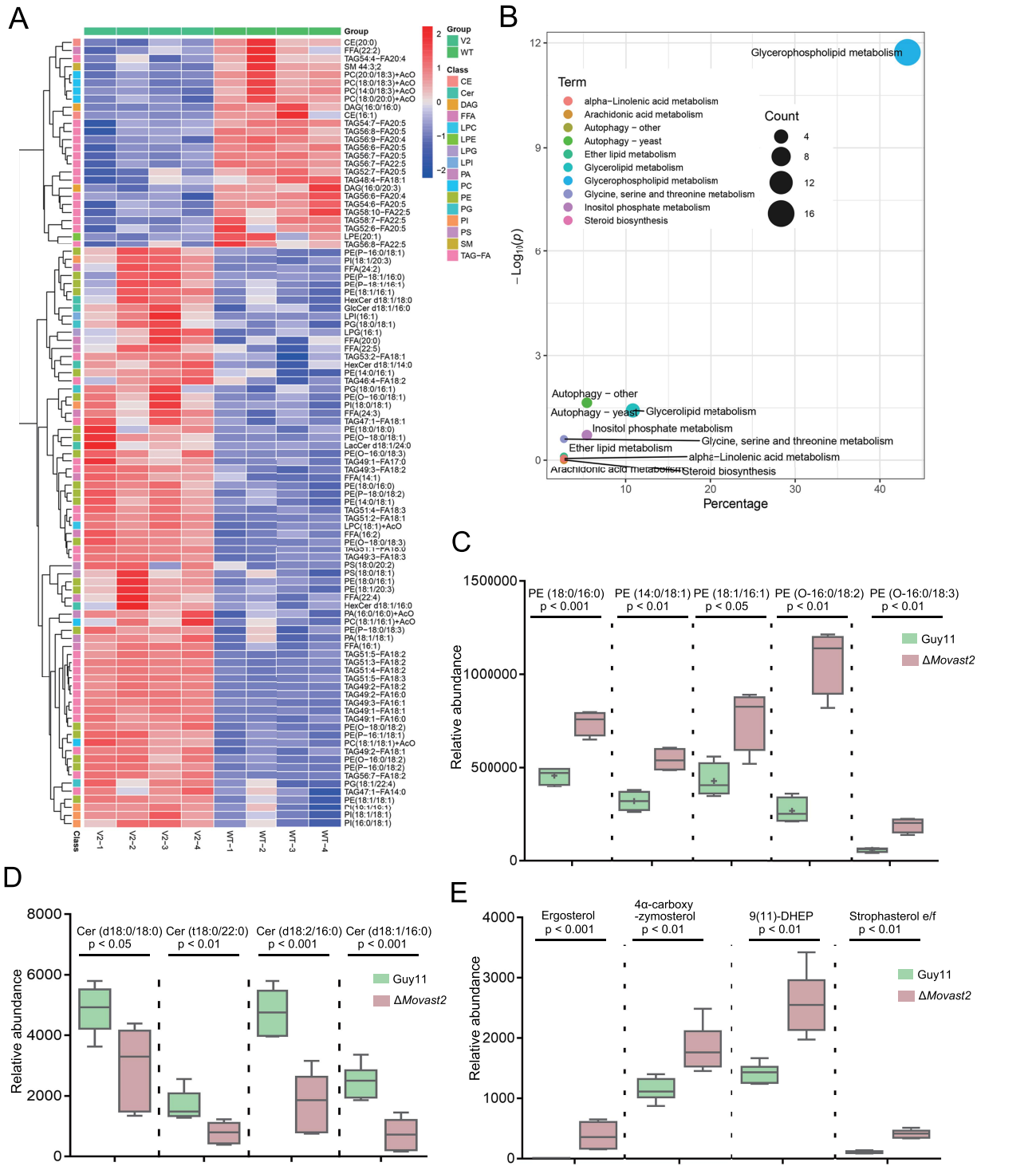

Figure 8. Lipidomics evaluated the lipids contents in Δ*Movast2*. (A) Heatmap showing the significantly different features in lipid profiles of Δ*Movast2* compared with the wild-type Guy11 strain (Red indicated higher and blue represented lower among these lipids). (B) KEGG enrichment analysis showed the significantly different lipids involved in autophagy, lipid metabolism, steroid biosynthesis and other lipid metabolism pathways. (C, D, E) The relative content of PE, Cer, and sterols was calculated using Prism 7.0.

MoVast2 and MoVast1 were redundant. To make this determination, we knocked out the *MoVAST1* gene in the Δ*Movast2* mutant and successfully obtained Δ*Movast1* Δ*Movast2* double mutants. However, the phenotype of Δ*Movast1* Δ*Movast2* was similar to Δ*Movast1* and no more severe characteristic was found (Fig. S4). We suspect an independent role or potential relationship between MoVast1 and MoVast2. Next, we transformed plasmids expressing GFP-MoVast2 and RFP-MoVast1 into the Guy11 strain to observe the localization between MoVast1 and MoVast2. In conidia, the green dots and red dots appeared after 2 h on the artificial inductive surface and the two fluorescent signals coincided completely (Figure 10A). We also observed the localization of MoVast1 and MoVast2 in the appressoria. At 12 hpi, the

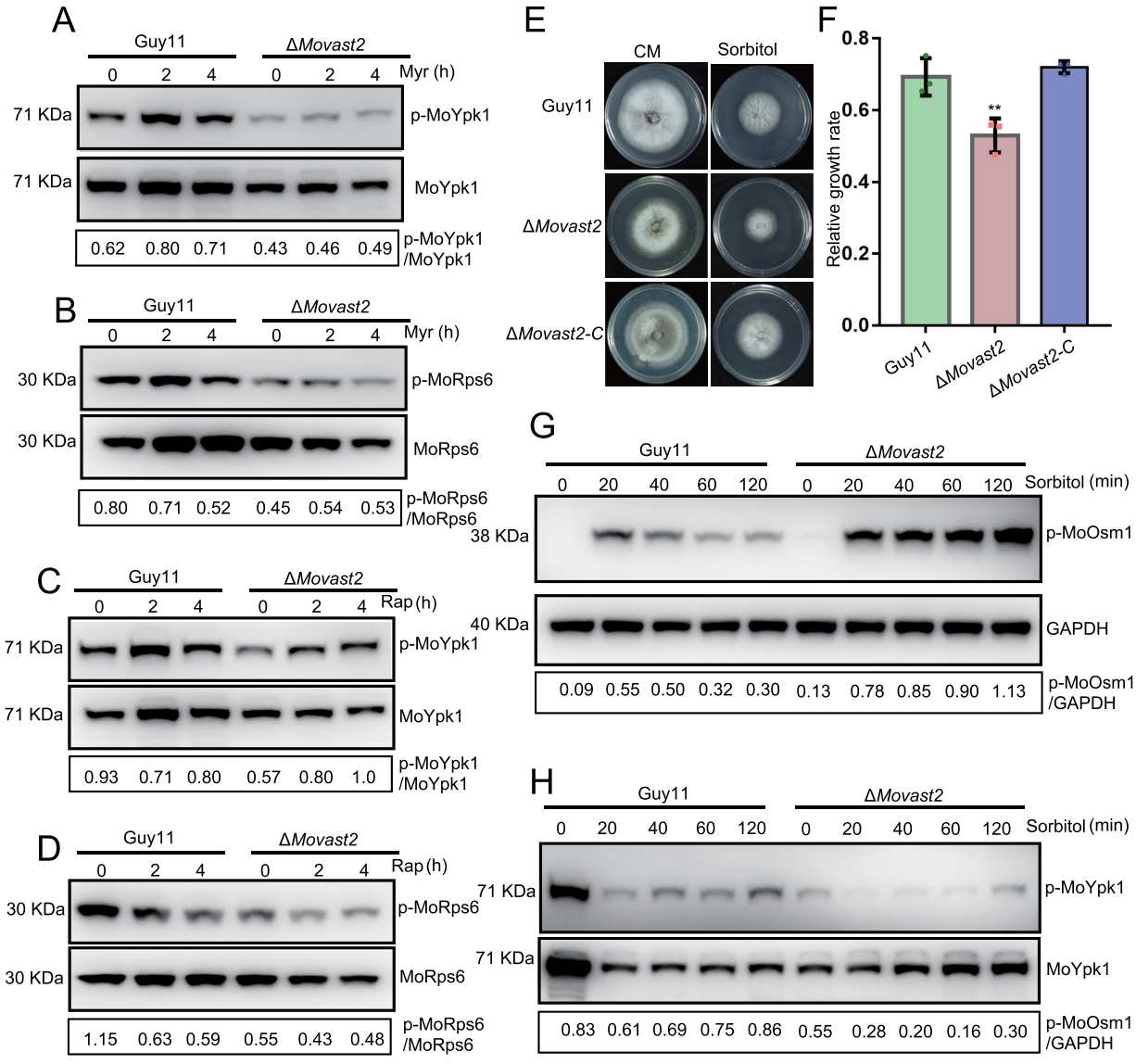

Figure 9. Both TORC1 and TORC2 are compromised in Δ*Movast2*. (A) Detection of TORC2 activity. The mycelia were cultured in CM medium for 2 days with the addition of 2 μM myriocin to induce for 2 and 4 h. The proteins were extracted by TCA-acetone-SDS and the phosphorylation of MoYpk1 was measured using MoYpk1 and p-MoYpk1 antibody. (B) The activity of TORC1 was detected when being treated with 2 μM myriocin for 2 and 4 h. (C) The phosphorylation level of MoYpk1 was assessed after treatment with 100 ng/ml rapamycin for 2 and 4 h. (D) The phosphorylation level of MoRps6 was measured after being treated with 100 ng/ml rapamycin for 2 and 4 h. (E) Hyperosmotic stress was implemented. The wild-type Guy11, Δ*Movast2*, and the complemented strain on CM medium and CM medium containing 1 M sorbitol were cultured for 7 days. (F) The relative growth rate was analyzed. Asterisks represent significant differences (** $p < 0.01$). (G) The phosphorylation level of MoOsm1 was detected when being treated with 1 M sorbitol for 20, 40, 60, and 120 min. (H) The activity of TORC2 was detected under hyper-osmotic stress conditions.

fluorescence gathered in the conidia and more punctate fluorescence appeared in the appressoria. At 24 hpi, both GFP-MoVast2 and RFP-MoVast1 disappeared in the conidia and the punctate fluorescence gathered in the appressoria. This localization condition also appeared in hypha (Figure 10B). These results demonstrated that MoVast1 and MoVast2 may cooperate to regulate the pathogenicity of *M. oryzae*.

To examine whether MoVast1 and MoVast2 undergo cross-talk in *M. oryzae*, we transformed GFP-MoVast1 into the Δ*Movast2* mutant and transformed GFP-MoVast2 into the Δ*Movast1* mutant. We found that the GFP-MoVast1 punctate fluorescence significantly decreased in the Δ*Movast2* mutant. However, neither the Δ*Movast1* mutant nor the wild-type strain Guy11 showed any differences for GFP-MoVast2 (Figure 10C, D).

The C terminus of MoVast2 is essential for its function

Previous studies found that the GRAM and VASt domain of MoVast1 have functions in conidiation, pathogenicity and localization. To explore the detailed functions of MoVast2, we constructed GFP-MoVast2, GFP-MoVast2(1–924) and GFP-MoVast2(1–1095) plasmids and transformed them into the Δ*Movast2* mutant. The GFP-MoVast2 strain completely restored the defects of Δ*Movast2*, whereas the GFP-MoVast2 (1–924) and GFP-MoVast2(1–1095) could not restore these defects (Fig. S5A, B). Next, we also observed the localization of GFP-MoVast2 in these strains. As expected, the GFP-MoVast2 strain displayed punctate fluorescence in conidia, while few puncta could be found in MoVast2(1–924) and

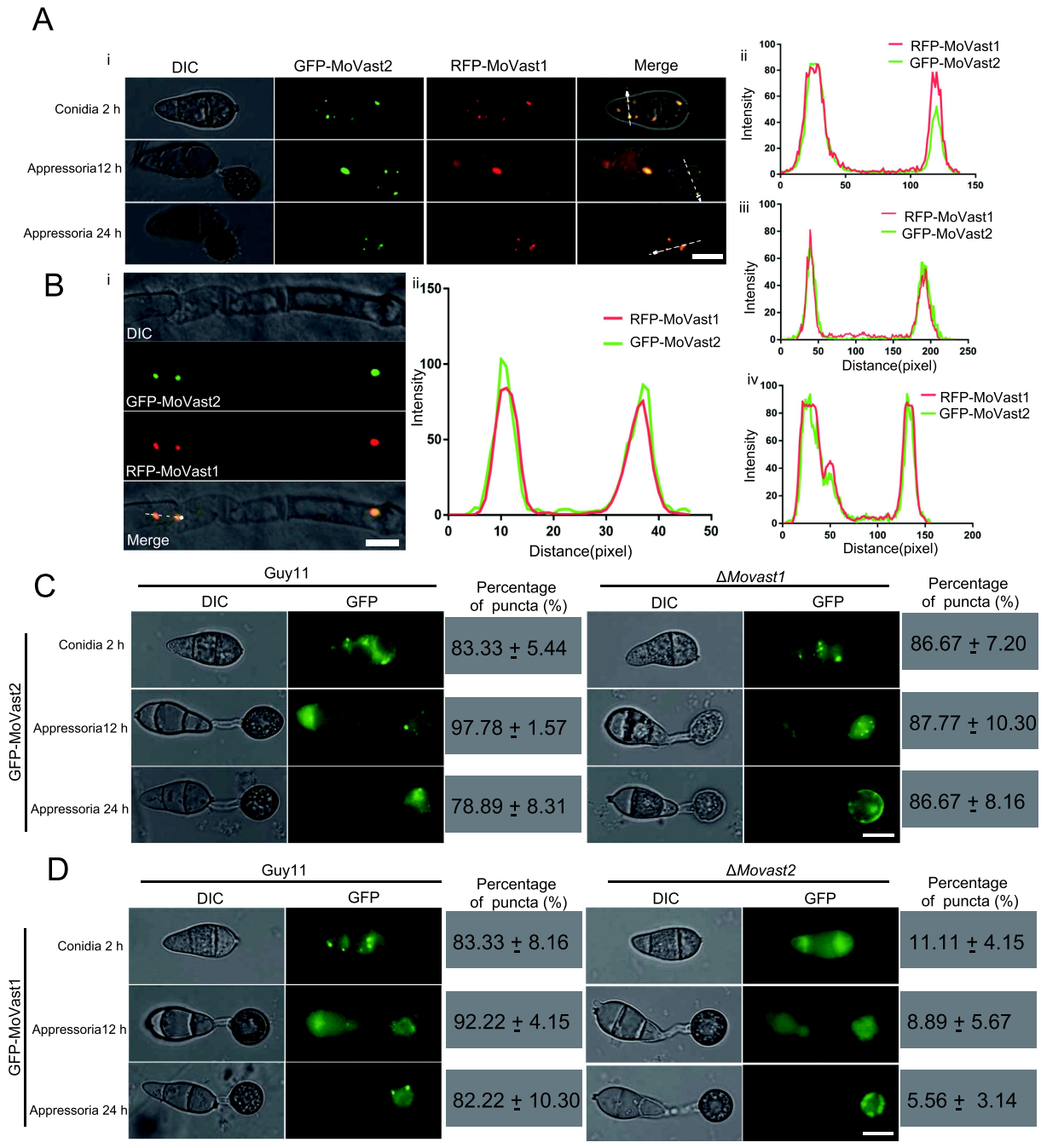

Figure 10. The localization of MoVast1 is disturbed in the Δ*Movast2* mutant. (A) The localization of MoVast1 and MoVast2 were observed during the appressorium formation stages. (I) The GFP-MoVast2 and RFP-MoVast1 were co-transformed into the wild-type strain and the localization conditions were observed using confocal microscopy. Bar: 10 μm. (ii–iv) Fluorescence densities of GFP-MoVast2 and RFP-MoVast1 in conidia, and appressoria at 12 h and 24 h were analyzed using ImageJ software. (Bi) The localization of MoVast1 and MoVast2 was observed in the mycelium. Bar: 10 μm. (Bii) Fluorescence densities of GFP-MoVast2 and RFP-MoVast1 in mycelium were measured using ImageJ software. (C) The localization of GFP-MoVast2 in the wild-type and Δ*Movast1* mutant. Bar: 10 μm. (D) The localization of GFP-MoVast1 in the wild-type and Δ*moVast2* mutant. Bar: 10 μm.

GFP-MoVast2(1–1095) (Fig. S5C). These results indicated that the C terminus of MoVast2 is essential for its function. As previous studies showed, the VASt domain of MoVast1 plays essential roles in conidiation, pathogenicity and localization. Thus, we further explored the C terminal functions of MoVast1. Unexpectedly, the deficiencies of Δ*Movast1* were nevertheless restored when the C terminus of that protein was lost (Fig. S5D). These results suggested that MoVast2 and MoVast1 play distinct functions in *M. oryzae*.

Discussion

Autophagy is a crucial cellular signaling process that is conserved across all eukaryotes, including fungi, plants, and animals

[49,50]. To ensure cell viability, the autophagy mechanism breaks down undesirable substances such as protein aggregates, damaged mitochondria, and even viruses [51–53]. In plant pathogenic fungi, autophagy proteins have been well studied in many species such as *M. oryzae, Fusarium graminearum, Ustilago maydis* and *Botrytis cinerea* [54–60]. In *M. oryzae*, the appressorium is a key infection structure that generates an enormous pressure of up to 8.0 Mpa in order to penetrate cell cuticles [31]. During the appressorium formation stage, the conidium is broken down by autophagy and the degraded materials are delivered to the appressorium to generate enormous pressure. Disruption of core autophagy proteins results in appressorium formation defects and loss of pathogenicity in *M. oryzae* [56]. Despite lacking a typical infection structure, autophagy is nonetheless necessary for *F. graminearum* to achieve full virulence and is even involved in toxin biosynthesis [61]. In recent years, some new regulators of autophagy were identified, such as the carbon responsive regulator MoAbl1, the glutaminolysis regulator MoAsd4, the deacetylation protein MoSnt2, and the sterol binding protein MoVast1, which have helped us better understand the autophagy regulation mechanism in plant pathogenic fungi [33]. In this study, we identified another autophagy regulator, MoVast2, in *M. oryzae*. Our studies showed that MoVast2 is involved in appressorium development and the activity of TORC1 and TORC2. MoVast2 is crucial for the functions of MoVast1 in cell localization and response to hyperosmotic stress.

TOR, as a highly conserved protein kinase, plays vital roles in many cell processes, such as cell growth, ribosome biogenesis, cell mitosis and autophagy [39,62–66]. In most eukaryotes, only a single gene exists, while some fungi such as yeast contain two TOR genes [67]. TOR assembles into two distinct multiprotein complexes, TORC1 and TORC2, in both yeast and animals [4,68–71]. The major regulators directing the transmission of cellular growth signals and the advancement of autophagy have previously been identified as TORC1 and are well understood. The roles of TORC2, however, received relatively little attention. Recent research has identified TORC2 as a key regulator for preserving cell surface homeostasis [4]. In pathogenic fungi, TOR signaling was also studied in recent years and was shown to play key roles in cell growth, cell mitosis, autophagy and virulence [40,41,72–77]. It is yet unknown how TOR controls these developments and if TORC1 and TORC2 are present in plant pathogenic fungi. Our previous studies found a sterol binding protein, MoVast1, which regulates PM sterol homeostasis to control PM tension and thereby coordinate the activity of TOR and autophagy in rice blast fungus [33]. In this study, we identified another VASt domain-containing protein, MoVast2, in *M. oryzae*. We found that MoVast2 also regulates the homeostasis of sterols and sphingolipid and contributes to fungal development and pathogenicity. When the content of sterols is excessively accumulated in the PM, MoVast1 will bind MoVast2 to transfer sterols from the PM to the ER. Meanwhile, the high level of sterols in the PM further promotes TORC2 activity to produce more sphingolipids and activate TORC1 to launch cell mitosis and cell growth. When the MoVast2 is disrupted, the sterol reflux is blocked, which results in a high concentration of sterol in the PM and causes huge intracellular stress, thereby downregulating TOR activity and activating autophagy (Figure 11). These findings first highlighted the functions of TORC1 and TORC2 in plant pathogenic fungi and then provided insight into the intricate processes by which MoVast1 and MoVast2 regulate *M. oryzae*.

In summary, this study identified another VASt domain-containing protein and analyzed the functions of MoVast2 in cell growth, appressorium development and the regulation mechanism in *M. oryzae*. MoVast2 has crucial functions in preserving PM homeostasis, TOR activity, and autophagy, just like MoVast1. Furthermore, we uncovered a critical link between MoVast2 and MoVast1 and MoAtg8. In *M. oryzae*, both MoVast2 and MoVast1 can interact with MoAtg8 at the PAS and the function of MoVast1 is dependent on MoVast2. Disruption of MoVast2 leads to mislocalization of MoVast1. Our research has further verified the specific functions of VASt-containing proteins in *M. oryzae*, and future work will examine the two VASt domain structures to create novel treatment approaches to combat the rice blast fungus.

Materials and methods

Generation of the mutant and complemented strains

In this study, the gene deletion strategy was based on homologous recombination of *Agrobacterium tumefaciens*-mediated transformation (*At*MT). The knockout vector was designed using PKO3A by Lu *et al*. as described previously [78]. Briefly, upstream and downstream fragments of MoVast2 of approximately 1000 bp were obtained separately by PCR with specific primers. Then the upstream gene fragment, the resistance gene fragment (*HPH/BAR/SUR*) and the downstream gene fragment were fused with cleaved PKO3A plasmids using recombinase exnase (Vazyme Biotech Co., Ltd, C113-02). The recombination cassettes were imported into the wild-type strain Guy11 using *Agrobacterium tumefaciens* C58 strain (AGL1; Shanghai Weidi Biotechnology Co., Ltd, AC1020) and the positive transformants were selected on complete medium (CM [33];) with 200 μg/mL hygromycin B (Sangon Biotech, A100607) and 0.5 μM 5-fluoro-2'-deoxyuridine (Sigma-Aldrich, F0503). The single-copy mutant was further verified by PCR and southern blot as previously described [33].

For southern blot analysis, the transformants were cultured in CM medium for 3 days and the whole DNA was extracted using CTAB buffer (50 mM CTAB [Sango Biotech, A600108], 1.4 M NaCl [Sango Biotech, A610476], 0.1 M Tris-HCl [Sango Biotech, B548127], 20 mM EDTA [Sango Biotech, B540625]). The digested whole DNA was labeled using the DIG-High Prime DNA Labeling and Detection Starter Kit II (Roche, 11,585,614,910) following the manufacturer's instructions [79].

Complemented strains with the PKD5-GFP/PKD3-GFP plasmid vector with the sulfonylurea resistance gene (*SUR*) were used [42]. The positive transformants were verified by western blot and fluorescence microscopy.

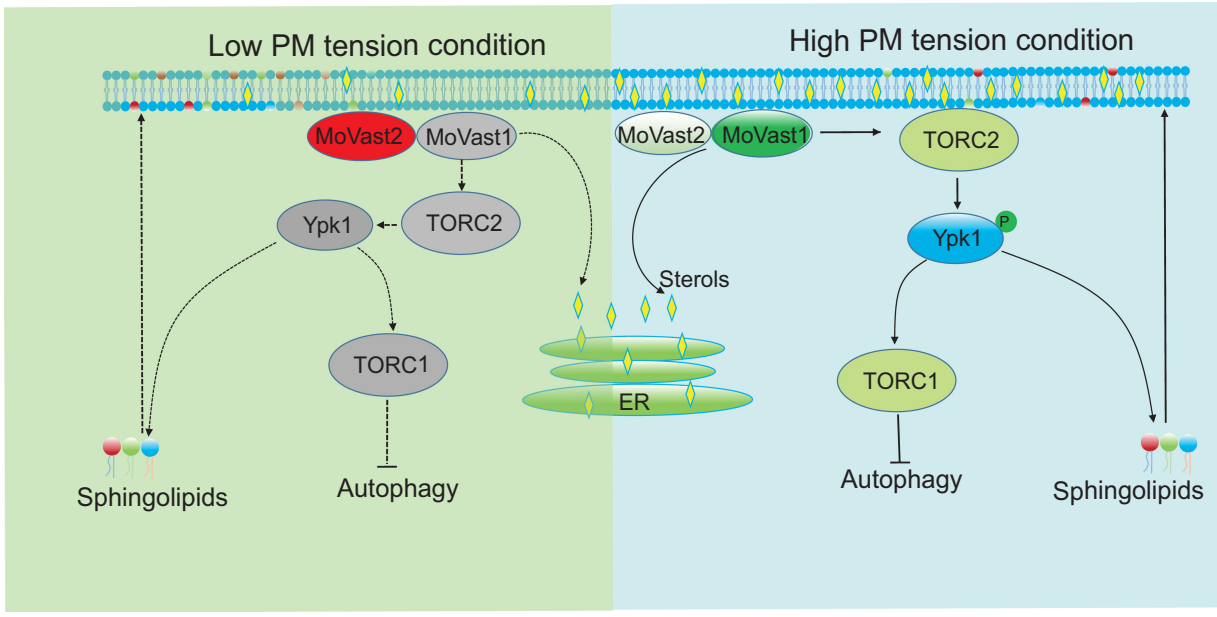

Figure 11. The regulation model of MoVast2 in *M. oryzae*. MoVast2 is another PM-binding protein, which interacts with MoVast1 to maintain PM homeostasis in *M. oryzae*. MoVast2 binds MoVast1 to respond to the PM tension and regulates the activity of both TORC1 and TORC2. When the content of sterols was excessively accumulated in the PM, MoVast1 will bind MoVast2 to transfer sterols from the PM to the ER. Meanwhile, the high level of sterols in the PM further promotes TORC2 activity to produce more sphingolipids and activate TORC1 to launch cell mitosis and cell growth.

Strains, culture conditions, and phenotypic analyses

The wild-type strain of *M. oryzae*, Guy11, was cultured on CM at 25°C under a 16–18 light-dark cycle [80]. For phenotypic analyses, the wild-type strain Guy11, the Δ*Movast2* mutant and the complemented strain Δ*Movast2-C* were cultured on CM for 7 days and then the colony diameter and conidia production were measured. For conidia germination and appressorium formation assays, the conidia were gathered and diluted to 1×10^5 conidia/mL and then dropped onto glass slides and artificial hydrophobic films, respectively. After incubation at 22°C for 4 h and 24 h, the germination and appressorium formation rate were observed and counted using a Nikon microscope Ti-80. For the virulence test, the mycelium plugs were incubated on cut leaves of barley and cultured for 4 days at 25°C. For rice incubation assay, the spore suspensions (1×10^5 conidia/mL) were sprayed on two-week-old rice seedlings (International Rice Research Institute/IRRI, CO39) and cultured at 22°C for 2 days and then transferred to 25°C for 3 days.

Growth stress assay

To test the response of mutants to rapamycin, myriocin and sorbitol inhibitors, 100 ng/ml rapamycin (APExBIO, A8167), 2 μM myriocin (APExBIO, B6064) and 1 M D-Sorbitol (Sangon Biotech, A100691) were added to the CM medium and the same concentration of DMSO as a control was added. The wild-type strain Guy11, the Δ*Movast2* mutant and the complemented strain Δ*Movast2-C* were incubated in the presence of these inhibitors and cultured for 7 days at 28°C in dark conditions. Every sample was repeated 3 times and the relative growth rates were calculated using the formula: growth rate = (the diameter of the strain treated with chemicals)/(the diameter of the untreated strain) [42].

Autophagy flux detection

To monitor autophagic flux, the GFP-MoAtg8 fragment with 1000 bp of upstream and downstream fragments were fused to the PKO3A vector and then introduced into the Guy11 and Δ*Movast2* mutant strains using *Agrobacterium tumefaciens*. The *in situ* transformants were verified by PCR and fluorescence microscopy. For the autophagy degradation assay, the wild-type strain Guy11 and the Δ*Movast2* mutant with GFP-MoAtg8 were cultured on CM medium for 7 days, then transferred to CM liquid medium and incubated at 150 rpm for 48 h at 25°C and transferred to SD-N medium for 2 and 4 h induction. Autophagosomes were observed by fluorescence microscopy with a green laser at 488 nm.

Immunoblotting analysis

For GFP-MoAtg8 detection, the mycelium was ground using liquid nitrogen and the proteins were extracted with protein lysis buffer (50 mM Tris-HCl, pH 7.6, 150 mM NaCl, 1% Triton X-100 [Sangon Biotech, A110694], 0.5 mM EDTA). The GFP and GFP-MoAtg8 fusion bands were detected with GFP antibody (1:10,000; Abcam, ab32146) after resolution on 4–12% gradient SDS-PAGE gels.

Phosphorylation level analysis

For phosphorylation level detection, the wild-type strain Guy11 and the Δ*Movast2* mutant were cultured in CM liquid

medium for 48 h at 25°C and the proteins were extracted by the TCA-acetone-SDS method. The phosphorylation level of Rps6 was examined by p-Rps6 and Rps6 antibody (Prepared by Abclonal Biotechnology Co., Ltd) and the phosphorylation level of MoYpk1 was examined by p-MoYpk1 and MoYpk1 antibody (Prepared by Abclonal Biotechnology Co., Ltd).

Wide-target lipidomic analysis

For lipidomic analysis, the wild-type and Δ*Movast2* strains were cultured in CM liquid medium at 25°C for 2 days, collected and dried using a freeze dryer. Two hundred μL of aqueous methanol (3:1, v:v) was added per 50 mg weight of sample and mixed with 1 mL of MTBE (methyl tert-butyl ether) at 4°C and shock extracted for 60 min; 200 μL of H2O was then added and left at room temperature for 10 min; after centrifugation at 4°C and 16,000 g for 20 min, the supernatant was taken and 200 μL of SDT was used to re-solubilize the precipitated protein for quantification. The relative content of each sample was calculated based on the amount of protein in the sample. The same quantitative supernatant was extracted from each sample for vacuum drying. The dried extracts were redissolved in 100 μL dichloromethane/methanol solution (1:1, v:v), centrifuged at 4°C at 20,000 g for 15 min, and the supernatant was taken for LC-MS/MS analysis. The wide-target lipidomics was performed by Bioprofile, and detailed instrument parameters are the same as in previous studies [81].

Cell membrane permeability analysis

The cell membrane permeability detection was performed using the method of Zhang et al. with slight modifications [82]. Briefly, the conidia of each sample were gathered and 6,010 g for 10 min. The precipitated conidia were resuspended with 1 ml PBS (Sango Biotech, B548117) and diluted to 1×10^7 conidia/ml. Then the cells were grown at 25°C for 24 h. After incubation, the samples were centrifuged at 9,391 g for 10 min, and the absorbance of the supernatant was read at 260/280 nm using a UV–vis spectrophotometer and the content of DNA and proteins was calculated.

Statistical analyses

The intensity of fluorescence was quantified using ImageJ software in fluorescence and immunoblot analysis. The results are presented as the mean ± standard deviation of at least three independent measurements. Statistical significance was determined using a two-sample Student's t-test, performed with GraphPad Prism version 7.0. The p-value was used to assess the statistical significance of the results.

Disclosure statement

Dr. Daniel J. Klionsky is a Founder and Editor-in-Chief of Autophagy. All authors declare no conflict of interest.

Funding

This study was supported by grants from the National Natural Science Foundation of China [32100159, 31970140 & 31972216], Key R&D projects of Zhejiang Province of China [2021C02010], Natural Science Foundation of Zhejiang province of China [LQ22C140005] and National Institutes of Health of USA [GM131919];Research and Development Project of Zhejiang Province [2021C2010];Natural Science Foundation of Zhejiang Province [LQ22C140005].

Abbreviations

ATMT: *Agrobacterium tumefaciens-mediated* transformation; BiFC: bimolecular fluorescence complementation; COP: coat protein; Co-IP: co-immunoprecipitation; CM: complete medium; ER: endoplasmic reticulum; HMM: hidden Markov models; hpi: post-inoculation; IH: invasive hyphae; MCC: membrane compartment occupied by Can1; MCT: membrane compartment containing TORC2; PAS: phagophore assembly site; PM: plasma membrane; SD-N: synthetic defined medium without amino acids and ammonium sulfate; TOR: target of rapamycin; VASt: VAD1 analog of StAR-related lipid transfer.

ORCID

Daniel J. Klionsky http://orcid.org/0000-0002-7828-8118
Fu-Cheng Lin http://orcid.org/0000-0002-4127-8143

References

[1] Berchtold D, Piccolis M, Chiaruttini N, et al. Plasma membrane stress induces relocalization of Slm proteins and activation of TORC2 to promote sphingolipid synthesis. Nat Cell Biol. 2012 May;14(5):542–547.
[2] Kusumi A, Fujiwara TK, Tsunoyama TA, et al. Defining raft domains in the plasma membrane. Traffic. 2020;21(1):106–137.
[3] Grosjean K, Mongrand S, Beney L, et al. Differential effect of plant lipids on membrane organization. J Biol Chem. 2015;290 (9):5810–5825.
[4] Riggi M, Kusmider B, Loewith R. The flipside of the TOR coin – TORC2 and plasma membrane homeostasis at a glance. J Cell Sci. 2020;133(9):jcs242040.
[5] A-L LR, Quiroga X, Walani N, et al. The plasma membrane as a mechanochemical transducer. Philos Trans R Soc B. 2019;374 (1779):20180221.
[6] Gulati S, Liu Y, Munkacsi AB, et al. Sterols and sphingolipids: dynamic duo or partners in crime? [Review]. Prog Lipid Res. 2010 Oct;49(4):353–365.
[7] Breslow DK, Weissman JS. Membranes in balance: mechanisms of Sphingolipid Homeostasis. Mol Cell. 2010;40(2):267–279.
[8] Guan XL, Souza CM, Pichler H, et al. Functional interactions between sphingolipids and sterols in biological membranes regulating cell physiology [Article]. Mol Biol Cell. 2009 Apr;20 (7):2083–2095.
[9] Lee JY, Marian OC, Don AS. Defective lysosomal lipid catabolism as a common pathogenic mechanism for dementia. Neuromolecular Med. 2021;23(1):1–24.
[10] Holthuis JCM, Pomorski T, Raggers RJ, et al. The organizing potential of sphingolipids in intracellular membrane transport [Review]. Physiol Rev. 2001 Oct;81(4):1689–1723.
[11] Bartlett K, Kim K. Insight into Tor2, a budding yeast microdomain protein [Review]. Eur J Cell Biol. 2014 Mar;93(3):87–97.
[12] Roelants FM, Leskoske KL, Marshall MNM, et al. The TORC2-dependent signaling network in the yeast *Saccharomyces cerevisiae* [Review]. Biomolecules. 2017 Sep;7(3):66.
[13] Topolska M, Roelants FM, Si EP, et al. TORC2-dependent Ypk1-mediated phosphorylation of Lam2/Ltc4 disrupts its association with the β-propeller protein Laf1 at endoplasmic Reticulum-

Plasma membrane contact sites in the yeast *Saccharomyces cerevisiae*. Biomolecules. 2020;10(12):1598.
[14] Lorrain S, Lina BQ, Auriac MC, et al. Vascular associated death1, a novel gram domain-containing protein, is a regulator of cell death and defense responses in vascular tissues. Plant Cell. 2004 Aug;16(8):2217–2232.
[15] Sandhu J, Li S, Fairall L, et al. Aster proteins facilitate nonvesicular plasma membrane to ER cholesterol transport in mammalian cells. Cell. 2018;175(2):514–529.e20.
[16] Jentsch J-A, Kiburu I, Pandey K, et al. Structural basis of sterol binding and transport by a yeast StARkin domain. J Biol Chem. 2018 Apr 13;293(15):5522–5531.
[17] van Meer G, Voelker DR, Feigenson GW. Membrane lipids: where they are and how they behave [Review]. Nat Rev Mol Cell Biol. 2008 Feb;9(2):112–124.
[18] Radhakrishnan A, Goldstein JL, McDonald JG, et al. Switch-like control of SREBP-2 transport triggered by small changes in ER cholesterol: a delicate balance [Article]. Cell Metab. 2008 Dec 3;8(6):512–521.
[19] Holthuis JCM, Menon AK. Lipid landscapes and pipelines in membrane homeostasis. Nature. 2014;510(7503):48–57.
[20] Guo Z, Liu X, Wang N, et al. Membrane component ergosterol builds a platform for promoting effector secretion and virulence in Magnaporthe oryzae. New Phytol. 2023 Oct;237(3):930–943.
[21] Funato K, Riezman H, Muniz M. Vesicular and non-vesicular lipid export from the ER to the secretory pathway [Article]. Biochimica Et Biophysica Acta-Molecular and Cell Biology of Lipids. 2020 Jan;1865(1):158453.
[22] Georgiev AG, Sullivan DP, Kersting MC, et al. Osh proteins regulate membrane sterol organization but are not required for sterol movement between the ER and PM [Article]. Traffic. 2011 Oct;12(10):1341–1355.
[23] Khafif M, Cottret L, Balague C, et al. Identification and phylogenetic analyses of VASt, an uncharacterized protein domain associated with lipid-binding domains in Eukaryotes. Bmc Bioinformatics. 2014 Jun;15(1):1–12.
[24] Bouchez O, Huard C, Lorrain S, et al. Ethylene is one of the key elements for cell death and Defense response control in the Arabidopsis lesion mimic mutant vad1. Plant Physiol. 2007 Oct;145(2):465–477.
[25] Topolska M, Roelants FM, Si EP, et al. TORC2-dependent Ypk1-mediated phosphorylation of Lam2/Ltc4 disrupts its association with the beta-propeller protein Laf1 at endoplasmic reticulum-plasma membrane contact sites in the yeast *Saccharomyces cerevisiae*. Biomolecules. 2020 Dec;10(12):1598.
[26] Sokolov SS, Vorobeva MA, Smirnova AI, et al. LAM genes contribute to environmental stress tolerance but sensibilize yeast cells to azoles. Front Microbiol. 2020 Jan;11:38.
[27] Roelants FM, Chauhan N, Muir A, et al. TOR complex 2-regulated protein kinase Ypk1 controls sterol distribution by inhibiting StARkin domain-containing proteins located at plasma membrane endoplasmic reticulum contact sites. Mol Biol Cell. 2018 Aug 15;29(17):2128–2136.
[28] Gatta AT, Wong LH, Sere YY, et al. A new family of StART domain proteins at membrane contact sites has a role in ER-PM sterol transport. Elife. 2015 May;4:e07253.
[29] Wilson RA. Magnaporthe oryzae. Trends Microbiol. 2021 Jul;29(7):663-664.
[30] Foster AJ, Talbot NJ. Getting a grip on blast. Nat Microbiol. 2020;5(12):1457–1458.
[31] Talbot NJ. Appressoria. Curr Biol. 2019;29(5):R144–R146.
[32] Wilson RA, Talbot NJ. Under pressure: investigating the biology of plant infection by Magnaporthe oryzae. Nature Rev Microbiol. 2009;7(3):185–195.
[33] Zhu XM, Li L, Cai YY, et al. A VASt-domain protein regulates autophagy, membrane tension, and sterol homeostasis in rice blast fungus. Autophagy. 2021 Oct;17(10):2939–2961.
[34] Cheong H, Nair U, Geng J, et al. The Atg1 kinase complex is involved in the regulation of protein recruitment to initiate sequestering vesicle formation for nonspecific autophagy in *Saccharomyces cerevisiae* [Article]. Mol Biol Cell. 2008 Feb;19(2):668–681.
[35] Proikas-Cezanne T, Pfisterer SG. Assessing mammalian autophagy by WIPI-1/Atg18 puncta formation. In: Klionsky DJ, editor. Methods in enzymology. Vol. 452. Pasadena, California: Academic Press; 2009. p. 247–260.
[36] Valverde DP, Yu S, Boggavarapu V, et al. ATG2 transports lipids to promote autophagosome biogenesis. J Cell Biol. 2019;218(6):1787–1798.
[37] Sakata KT, Hashii K, Yoshizawa K, et al. Coordinated regulation of TORC2 signaling by MCC /eisosome-associated proteins, Pil1 and tetraspan membrane proteins during the stress response. Mol Microbiol. 2022;117(5):1227–1244.
[38] Mirdita M, Schütze K, Moriwaki Y, et al. ColabFold: making protein folding accessible to all. Nat Methods. 2022;19(6):679–682.
[39] Jung CH, Ro S-H, Cao J, et al. mTOR regulation of autophagy. FEBS Lett. 2010 Apr 2;584(7):1287–1295.
[40] Qian B, Liu X, Ye Z, et al. Phosphatase-associated proteinMoTip41interacts with the phosphataseMoPpe1to mediate crosstalk betweenTORand cell wall integrity signalling during infection by the rice blast fungusMagnaporthe oryzae. Environ Microbiol. 2021 Feb;23(2):791–809.
[41] Qian B, Liu X, Jia J, et al. MoPpe1 partners with MoSap1 to mediate TOR and cell wall integrity signalling in growth and pathogenicity of the rice blast fungus Magnaporthe oryzae. Environ Microbiol. 2018 Nov;20(11):3964–3979.
[42] Zhu X, Li L, Wang J, et al. Vacuolar protein-sorting receptor MoVps13 regulates conidiation and pathogenicity in rice blast fungus magnaporthe oryzae. J Fungi. 2021;7(12):1084.
[43] Breslow DK, Collins SR, Bodenmiller B, et al. Orm family proteins mediate sphingolipid homeostasis. Nature. 2010;463(7284):1048–1053.
[44] Muir A, Ramachandran S, Roelants FM, et al. TORC2-dependent protein kinase Ypk1 phosphorylates ceramide synthase to stimulate synthesis of complex sphingolipids. eLife. 2014;3:e03779.
[45] Riggi M, Niewola-Staszkowska K, Chiaruttini N, et al. Decrease in plasma membrane tension triggers PtdIns(4,5)P2 phase separation to inactivate TORC2. Nat Cell Biol. 2018;20(9):1043–1051.
[46] Hohmann S. Control of high osmolarity signalling in the yeast *Saccharomyces cerevisiae*. FEBS Lett. 2009;583(24):4025–4029.
[47] Brewster JL, Gustin MC. Hog1: 20 years of discovery and impact. Sci Signal. 2014 Sep;7(343):re7.
[48] Liu X, Zhou Q, Guo Z, et al. A self-balancing circuit centered on MoOsm1 kinase governs adaptive responses to host-derived ROS in Magnaporthe oryzae. eLife. 2020;9:e61605.
[49] Liu X-H, Xu F, Snyder JH, et al. Autophagy in plant pathogenic fungi. Seminars in Cell & Developmental Biology. 2016;57:128–137.
[50] Walker SA, Ktistakis NT. Autophagosome Biogenesis Machinery. J Mol Biol. 2020 Apr 3;432(8):2449–2461.
[51] Xie Y, Kang R, Sun X, et al. Posttranslational modification of autophagy-related proteins in macroautophagy. Autophagy. 2015 Jan;11(1):28–45.
[52] Szatmari Z, Sass M. The autophagic roles of Rab small GTPases and their upstream regulators A review. Autophagy. 2014 Jul;10(7):1154–1166.
[53] Hale AN, Ledbetter DJ, Gawriluk TR, et al. Autophagy Regulation and role in development. Autophagy. 2013 Jul 1;9(7):951–972.
[54] Shen Z-F, Li L, Zhu X-M, et al. Current opinions on mitophagy in fungi. Autophagy. 2022:1-11.
[55] Liu X-H, Gao H-M, Xu F, et al. Autophagy vitalizes the pathogenicity of pathogenic fungi. Autophagy. 2012 Oct;8(10):1415–1425.
[56] Kershaw MJ, Talbot NJ. Genome-wide functional analysis reveals that infection-associated fungal autophagy is necessary for rice blast disease. Proceedings of the National Academy of Sciences. 2009;106(37):15967–15972.
[57] Yin Z, Chen C, Yang J, et al. Histone acetyltransferase MoHat1 acetylates autophagy-related proteins MoAtg3 and MoAtg9 to

orchestrate functional appressorium formation and pathogenicity in Magnaporthe oryzae. Autophagy. 2019;15(7):1234–1257.
[58] He M, Xu Y, Chen J, et al. MoSnt2-dependent deacetylation of histone H3 mediates MoTor-dependent autophagy and plant infection by the rice blast fungus Magnaporthe oryzae. Autophagy. 2018;14(9):1543–1561.
[59] Nadal M, Gold SE. The autophagy genes atg8 and atg1 affect morphogenesis and pathogenicity in Ustilago maydis. Mol Plant Pathol. 2010;11(4):463–478.
[60] Ren W, Sang C, Shi D, et al. Ubiquitin-like activating enzymes BcAtg3 and BcAtg7 participate in development and pathogenesis of Botrytis cinerea. Curr Genet. 2018;64(4):919–930.
[61] Lv W, Wang C, Yang N, et al. Genome-wide functional analysis reveals that autophagy is necessary for growth, sporulation, deoxynivalenol production and virulence in Fusarium graminearum. Sci Rep. 2017;7(1):1–12.
[62] Wang RC, Levine B. Autophagy in cellular growth control. FEBS Lett. 2010 Apr 2;584(7):1417–1426.
[63] Hands SL, Proud CG, Wyttenbach A. mTOR's role in ageing: protein synthesis or autophagy? Aging (Albany NY). 2009 Jul;1(7):586–597.
[64] Diaz-Troya S, Perez-Perez ME, Florencio FJ, et al. The role of TOR in autophagy regulation from yeast to plants and mammals. Autophagy. 2008 Oct 1;4(7):851–865.
[65] Kamada Y, Sekito T, Ohsumi Y. Autophagy in yeast: a TOR-mediated response to nutrient starvation. In: Thomas G, Sabatini DM, Hall MN, editors. Tor-target of rapamycin. current topics in microbiology and immunology. Vol. 2792003. Berlin Heidelberg: Springer-Verlag; 2004. p. 73–84.
[66] Manifava M, Smith M, Rotondo S, et al. Dynamics of mTORC1 activation in response to amino acids. eLife. 2016;5:e19960.
[67] Díaz-Troya S, Pérez-Pérez ME, Florencio FJ, et al. The role of TOR in autophagy regulation from yeast to plants and mammals. Autophagy. 2008;4(7):851–865.
[68] Toyoda Y, Saitoh S. Fission yeast TORC2 signaling pathway ensures cell proliferation under glucose-limited, nitrogen-replete conditions. Biomolecules. 2021 Oct;11(10):1465.
[69] Babst M. Eisosomes at the intersection of TORC1 and TORC2 regulation. Traffic. 2019 Aug;20(8):543–551.
[70] Gaubitz C, Prouteau M, Kusmider B, et al. TORC2 structure and function. Trends Biochem Sci. 2016 Jun;41(6):532–545.
[71] Otsubo Y, Yamamato M. TOR signaling in fission yeast. Crit Rev Biochem Mol Biol. 2008;43(4):277–283.
[72] Sun G, Qi X, Wilson RA, et al. Emerging from integrated TOR- and cAMP/PKA-signaling architecture reinforces magnaporthe oryzae appressorium morphogenesis. Mol Plant-Microbe Interact. 2019 May;32(5):593–607.
[73] Sun G, Elowsky C, Li G, et al. TOR-autophagy branch signaling via Imp1 dictates plant-microbe biotrophic interface longevity. PLoS Genet. 2019 Feb;15(2):e1008016.
[74] Marroquin-Guzman M, Sun G, Wilson RA. Glucose-ABL1-TOR signaling modulates cell cycle tuning to control terminal appressorial cell differentiation. PLoS Genet. 2017 Jan;13(1):e1006557.
[75] Marroquin-Guzman M, Wilson RA. Role of GATA transcription factors during infection of the rice blast fungus Magnaporthe oryzae. Phytopathology. 2015 Nov;105(11):89-89.
[76] Marroquin-Guzman M, RA W. GATA-dependent glutaminolysis drives appressorium formation in magnaporthe oryzae by suppressing TOR inhibition of cAMP/PKA signaling. PLoS Pathog. 2015 Apr;11(4):e1004851.
[77] Fernandez J, Marroquin-Guzman M, Wilson RA. Evidence for a transketolase-mediated metabolic checkpoint governing biotrophic growth in rice cells by the blast fungus magnaporthe oryzae. PLoS Pathog. 2014 Sep;10(9):e1004354.
[78] Zhu S, Yan Y, Qu Y, et al. Role refinement of melanin synthesis genes by gene knockout reveals their functional diversity in Pyricularia oryzae strains. Microbiol Res. 2021;242:126620.
[79] Liu X-H, Lu J-P, Zhang L, et al. Involvement of a Magnaporthe grisea serine/threonine kinase gene, MgATG1, in appressorium turgor and pathogenesis [Article]. Eukaryot Cell. 2007;Jun;6(6):997–1005.
[80] Talbot NJ, Ebbole DJ, Hamer JE. Identification and characterization of MPG1, a gene involved in pathogenicity from the rice blast fungus Magnaporthe grisea. Plant Cell. 1993 Nov;5(11):1575–1590.
[81] Yongxin Y, Nan Z, Xiaowei Z, et al. Metabolomic biomarkers identify differences in milk produced by Holstein cows and other minor dairy animals. J Proteomics. 2016;136:174–182.
[82] Zhang M, Lu J, Duan X, et al. Rimonabant potentiates the antifungal activity of amphotericin B by increasing cellular oxidative stress and cell membrane permeability [Article]. FEMS Yeast Res. 2021 May;21(3):foab016.